






Review

Broadband Time Domain Diffuse Optical Reflectance Spectroscopy: A Review of Systems, Methods, and Applications

Sanathana Konugolu Venkata Sekar ^{1,2,*}, Pranav Lanka ¹, Andrea Farina ³,
Alberto Dalla Mora ¹, Stefan Andersson-Engels ^{2,4}, Paola Taroni ^{1,3} and Antonio Pifferi ^{1,3,*}

¹ Dipartimento di Fisica, Politecnico di Milano, 20133 Milano, Italy; sriramapranav.lanka@polimi.it (P.L.); alberto.dallamora@polimi.it (A.D.M.); paola.taroni@polimi.it (P.T.)

² Biophotonics@Tyndall, IPIC, Tyndall National Institute, Lee Maltings, Dyke Parade, T12R5CP Cork, Ireland; stefan.andersson-engels@tyndall.ie

³ Consiglio Nazionale delle Ricerche, Istituto di Fotonica e Nanotecnologie, 20133 Milano, Italy; andrea.farina@polimi.it

⁴ Department of Physics, University College Cork, College Road, T12 K8AF Cork, Ireland

* Correspondence: sanathana.konugolu@tyndall.ie (S.K.V.S.); antonio.pifferi@polimi.it (A.P.); Tel.: +353-21-234-6606 (S.K.V.S. & A.P.)

Received: 22 October 2019; Accepted: 28 November 2019; Published: 12 December 2019



Abstract: This review presents recent developments and a wide overview of broadband time domain diffuse optical spectroscopy (TD-DOS). Various topics including physics of photon migration, advanced instrumentation, methods of analysis, applications covering multiple domains (tissue chromophore, in vivo studies, food, wood, pharmaceutical industry) are elaborated. The key role of standardization and recent studies in that direction are discussed. Towards the end, a brief outlook is presented on the current status and future trends in broadband TD-DOS.

Keywords: biomedical optics; time-of-flight; diffuse optics; NIR spectroscopy; broadband; in vivo; biophotonics; photon migration; time domain

1. Introduction

The study of the propagation of light in highly scattering media has great importance in a wide range of applications (biological media, pharmaceutical, food, wood) [1–6]. Over the last decade, advancements in instrumentation and novel methods of analysis and methodologies have fostered innovation and breakthroughs in diffuse optical spectroscopy (DOS) [7–9]. In particular, probing human tissue with light brings in a slew of benefits thanks to non-invasiveness, the potential for compact bedside or wearable monitoring, and cost-effective solutions [10–12]. That makes diffuse optics an attractive tool to explore the human body in vivo [12–15]. To harvest maximum benefit, various practical implementation approaches have been developed by the scientific community. Typically, the measurement scheme includes a light source and a detector placed at a known distance, and the acquired data are processed using diffusion models to extract the optical properties (absorption, scattering) of the medium under investigation. The continuous wave (CW) approach uses CW light sources to estimate optical properties [16–19]. Thus, only light attenuation is measured. This approach is easier to implement and cost-effective. However, it suffers from the coupling between absorption and scattering properties that cannot be independently evaluated from a single measurement. The solution to the coupling could be found by adding another dimension to the measurement. That can be achieved performing CW measurements at multiple source-detector distances or a different approach: frequency domain (FD) and time domain (TD): frequency domain (FD) and time domain (TD) acquire photon

propagation in diffusive media at multiple frequency and time, respectively [20–24]. Both approaches naturally disentangle the absorption and scattering coupling. The time domain approach has the advantage of gating photons at a different time of arrival, thus enabling depth segmentation of diffusive media based on the concept that longer propagation times allow photons to reach deep within the medium. *In vivo* applications of diffuse optics are mostly explored in the therapeutic window (600–1100 nm), where light attenuation in human tissues is comparatively low [25–28]. Furthermore, quantification of tissue constituents (chromophores) can be performed through the Beer–Lambert law, by a linear fit of typical tissue constituent absorption spectra with the broadband absorption spectrum of *in vivo* tissue [29,30]. Information on the microscopic structure, useful for tissue characterization, can also be derived from the scattering properties. Over the years, broadband diffuse optical spectroscopy using the above-mentioned approaches has been explored by various scientific communities across various applications, which, as mentioned initially, range from human tissue, to food, wood, pharmaceutical, and other [28,31–35].

This review will focus on the broadband time domain approach to diffusive media, henceforth named as time domain diffuse optical spectroscopy (TD-DOS). Unlike few wavelength time domain systems, broadband TD-DOS has the unique advantage of resolving an extended spectral range along with inherent benefits of depth segmentation using time gating and uncoupling of absorption from scattering. It is thus an ideal tool for exploration studies, where the key features of the tissue under study are understood, and the results, in turn, are exploited to create few wavelengths (typically smaller, cheaper, and simpler) dedicated systems [27,36–39]. With the advent of new technologies, the complexity of time domain instruments has been reduced from laboratory to compact devices, portable on wheels [23,27,36,40]. For the light source, bulky Ti:Sapphire lasers have been replaced by compact supercontinuum sources [41,42]. Robust and efficient solid-state detectors, like SPADs (single-photon avalanche diodes) or SiPMs (silicon photomultipliers) [43–46] have replaced delicate and fragile photomultiplier-based detection systems. A large addition of various data analysis methods of broadband time domain diffuse optics has been introduced to make the analysis simpler, accurate, and repeatable, thus providing a reliable method to analyze experimental data [47,48]. These new tools have opened up the scientific community to pursue standardization approaches that would validate and consolidate the data collection methodology and analysis methods, thus bringing in a harmonized approach across laboratories [49–51]. On the *in vivo* side, broadband TD-DOS is aptly placed to explore non-invasively new tissue locations and provide new insights on human physiological and pathological pathways. In this direction, various explorations have been conducted to characterize organs like breast, bone, thyroid, manubrium, forehead, brain, and others [13,23,26,29,52,53].

This review will provide a broad overview of the history and recent advancements of broadband TD-DOS as shown in the timeline Figure 1, covering the following aspects:

1. Physics of photon migration,
2. Broadband TD-DOS Instrumentation,
3. Analysis methods of TD-DOS,
4. Applications,
5. Future prospects.

The first part, the physics of photon migration, provides the fundamentals of temporal propagation of photons in highly scattering media. The gamut of broadband TD-DOS instruments and advancements is discussed in the second section. The next section elaborates on various analysis methods and methodologies to extract optical properties and estimate tissue constituents. A wide range of broadband TD-DOS applications is covered across various domains (tissue constituent characterization, *in vivo* studies, food, wood, standardization techniques) are deeply elaborated in this section. A brief summary on the future prospects of the broadband TD-DOS is presented at the end.

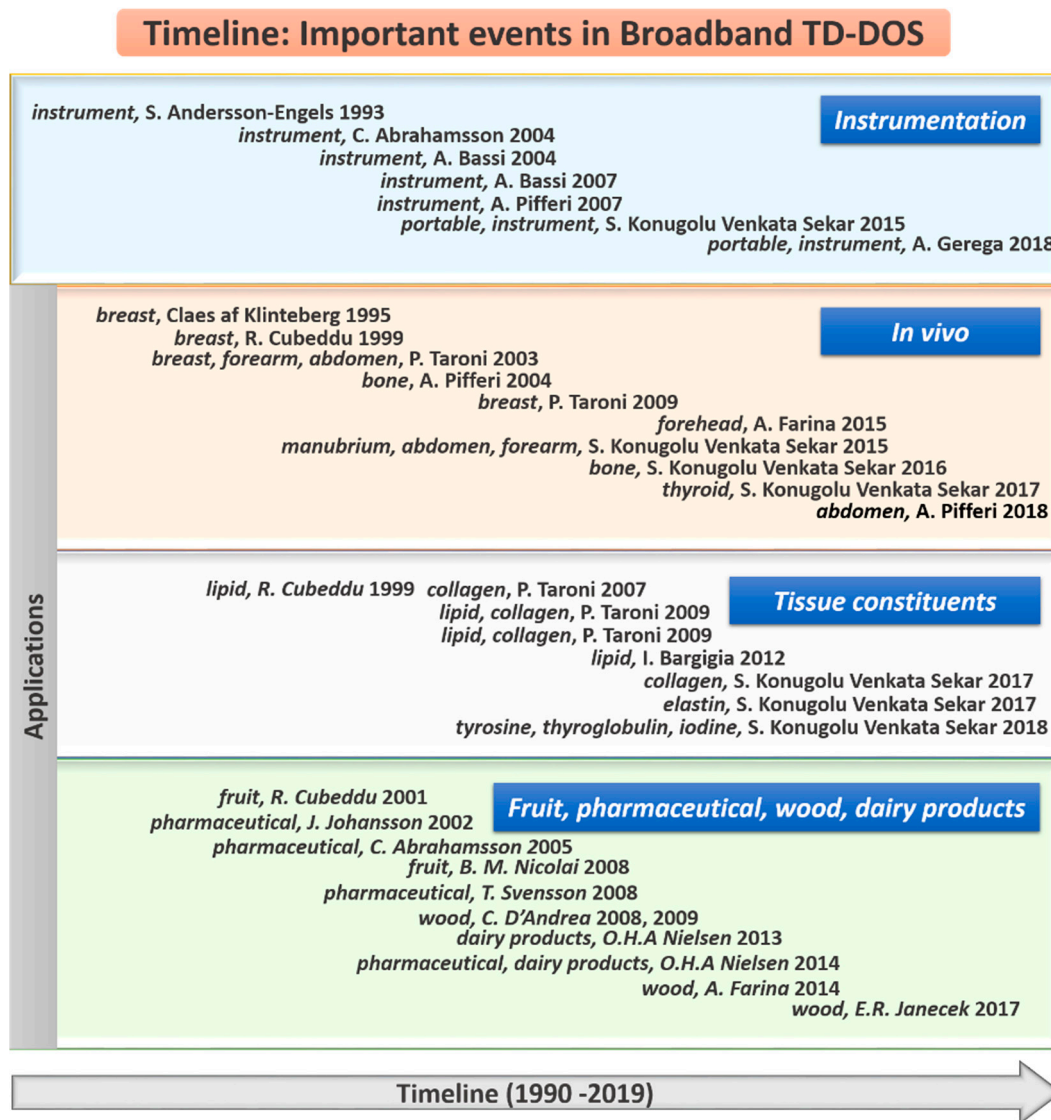


Figure 1. Timeline of important events to exemplify the evolution and potential of broadband time domain diffuse optical spectroscopy (TD-DOS): the top section shows the events in the advancement of instrumentation and the bottom three sections cover various applications of broadband TD-DOS.

2. Physics of Time Domain Diffuse Optical Spectroscopy (TD-DOS)

The photon propagation in a diffusive medium can be described by the radiative transfer equation (RTE), originally developed to describe the transport of non-interacting neutrons in nuclear science [54]. The assumption of non-interacting photons is still valid because, inside a diffusive medium, a multiple scattering regime is present, and consequently the light coherence vanishes after a few scattering events. Hereafter the RTE equation:

$$\frac{1}{v} \frac{\partial L}{\partial t} = -\mathbf{s} \cdot \nabla L(\mathbf{r}, \mathbf{s}, t) - (\mu_a + \mu_s)L(\mathbf{r}, \mathbf{s}, t) + \mu_s \int_{4\pi} p(\mathbf{s}, \mathbf{s}') L(\mathbf{r}, \mathbf{s}', t) d\mathbf{s}' + Q(\mathbf{r}, \mathbf{s}, t), \quad (1)$$

where $L(\mathbf{r}, \mathbf{s}, t)$ is the radiance at the position \mathbf{r} , which is the power flowing in the direction of the unit vector \mathbf{s} , per unit of solid angle and area normal to \mathbf{s} . v is the photon velocity in the medium, μ_a and μ_s are the absorption and scattering coefficients, $p(\mathbf{s}, \mathbf{s}')$ is the scattering phase function, which gives the probability that a photon running in the direction \mathbf{s} is scattered to the direction \mathbf{s}' , and $Q(\mathbf{r}, \mathbf{s}, t)$ is the spatial, temporal, and angular distribution of the source [55].

When a short pulse is injected in a diffusive medium and detected on the external surface, Equation (1), together with proper boundary conditions, rules the distribution of the photon time-of-flight (DTOF) after injection of a short pulse. The DTOF is related both to the volume probed by the light in the medium and to its optical properties (μ_a and μ_s). In fact, photons having travelled long paths give information on a larger volume than photon having travelled short paths (Figure 2). This fact is key for detecting information from deep regions of a tissue when the source and detector are placed on the surface on the same side, which is the most used configuration for non-invasive monitoring of biological tissues [56].

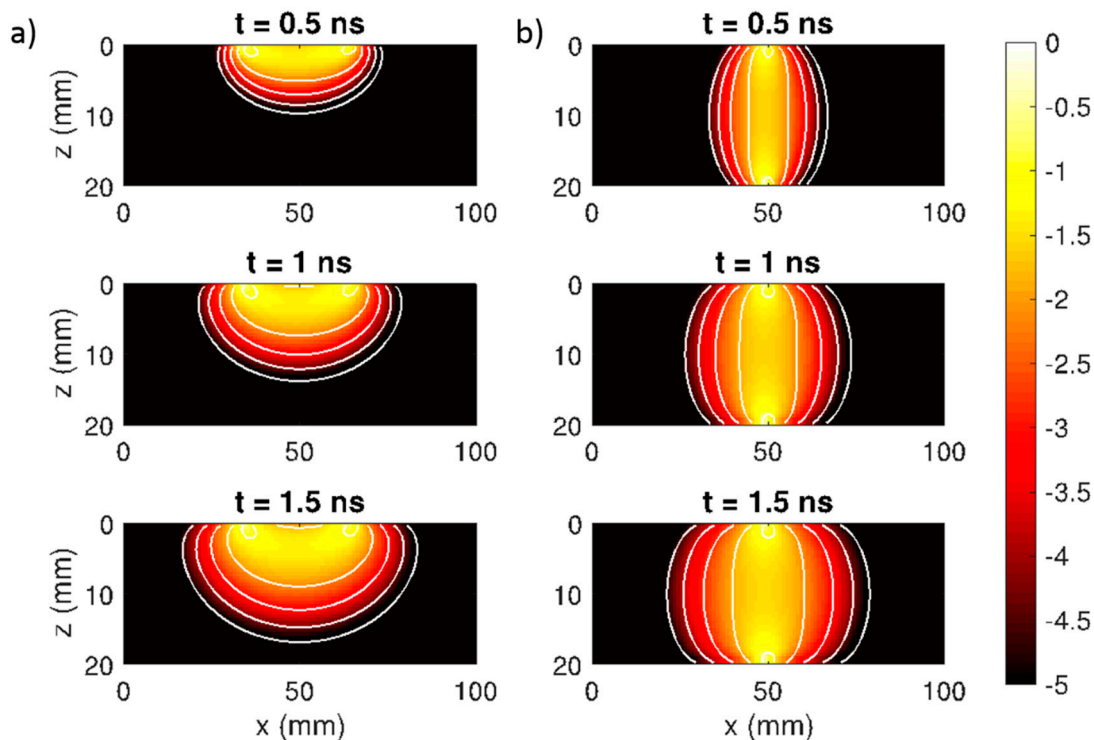


Figure 2. Sensitivity profiles (log 10), which represent the relative change in the detected signal when a localized defect is placed at every position of the volume, in a homogeneous diffusive medium. At three time intervals (0.5, 1, 1.5 ns) for: (a) reflectance geometry (3 cm source-detector distance) and (b) collinear transmittance geometry. Each white line represents the contour edge of the contrast every decade.

Another interesting advantage of the time domain approach is the fact that the shape of the DTOF is strongly modified by the absorption and scattering properties of the probed portion of the medium. Photons running a long path in the medium carry information about the probability of absorption, thus affecting the tail of the DTOF (Figure 3a). Instead, photons running a short path are more sensitive to the scattering properties of the medium, thus modifying the temporal position of the barycenter of the DTOF (Figure 3b).

These two effects open the possibility to estimate the spatial distribution of both optical properties (μ_a and μ_s) simultaneously from the shape of time-resolved DTOF using analytical, numerical, or stochastic models. Another advantage of such an approach relies on the fact that the estimation is unaffected by the amplitude of the DTOF, thus rejecting every source of error related to the optical coupling between tissue and delivery and/or detection optics.

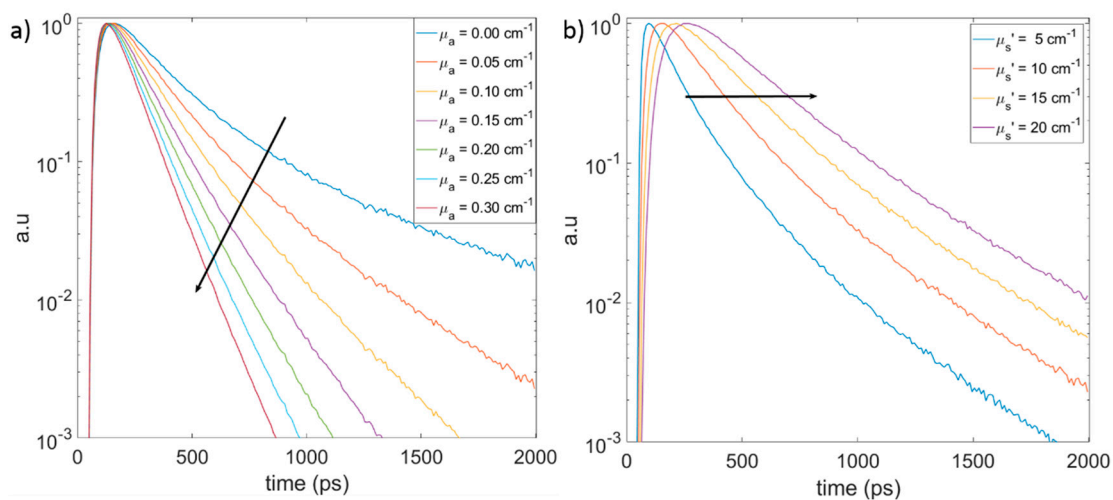


Figure 3. Monte Carlo simulations on a homogeneous semi-infinite medium in reflectance geometry. The source and detector separation is 1.5 cm. Effect of (a) absorption, with the arrow showing the increase in the slope of the distribution of the photon time-of-flight (DTOF) curves with increasing absorption and (b) scattering, with the arrow showing the shift in the peak position of DTOF with increasing scattering.

3. Instrumentation/Technology for Broadband TD-DOS

The key technical challenges for time domain diffuse optical spectrometry reside in the need to cover a wide spectral range with high sensitivity, down to the single-photon level, and with picosecond temporal resolution. Two different approaches can be envisaged to perform spectroscopy, which is either a sequential scheme, where the laser emitting wavelength within a relatively narrow (<10 nm) band is scanned progressively over the entire spectral range, or a parallel scheme, where the whole spectral range is acquired simultaneously. On the source side, a laser covering a wide spectral range is needed together with—for sequential wavelength scanning—a proper mechanism for filtering the desired wavelength out of a broad emission or alternatively a pulsed tunable laser. Furthermore, when the application involves biological media, a reasonably short total measurement time is also a must. Different realizations have been proposed in the course of the last decades, based on technical advancements mainly in the generation of supercontinuum laser sources and of time-correlated single-photon counting (TCSPC) detection [57].

The very first demonstration of broadband TD-DOS was realized by exploiting the white light generated from a water cell by a focused 10 Hz amplified laser pulse and a streak-camera for detection [58]. This setup was used to acquire the first in vivo absorption and reduced scattering spectra of the female breast in the 650–820 nm range [59]. In the first realization, a table-top amplified Ti:Sapphire laser was used as an injection source based on a 76 MHz femtosecond self-locking oscillator operated at 790 nm, followed by a pulse stretcher, a first-stage amplifier with intra-cavity dumping for reduction of the repetition rate to 10 Hz, a second stage multi-pass amplifier, and finally a pulse compressor. The outcome was a 10 Hz train of 200 fs pulses with 450 mJ energy, which were then focused onto a water cuvette to produce a white light pulsed emission, representing a considerable achievement at that time.

In a more recent realization (Figure 4) [60], the supercontinuum was generated into a 100 cm long photonic crystal fiber starting from a self-locked Ti:Sapphire laser. Light was injected into and collected from the sample under study using a couple of fibers for reflectance measurements or a free beam cell for transmittance measurements. Detection was achieved using an imaging spectrometer for spectral dispersion (Chromex, Model 250 IS) followed by a streak camera for temporal dispersion (Hamamatsu, Model C5680), resulting in 2D (wavelength-time) images projected onto a camera sensor. The key advantages of such an approach were the parallel spectral acquisition and the high temporal

resolution (ps) offered by the streak-camera. Also, the almost continuous acquisition over time and wavelength permitted adjustable optimization by slicing temporal and spectral photon distributions at post-processing. As limitations, we can quote the far-from-single-photon sensitivity of the detection, the non-linearity of both the temporal and spectral axes, the limited spectral range imposed by the poor quantum efficiency of the S1 photocathode in the streak-camera under use, and in general the cost/complexity of the workstation.

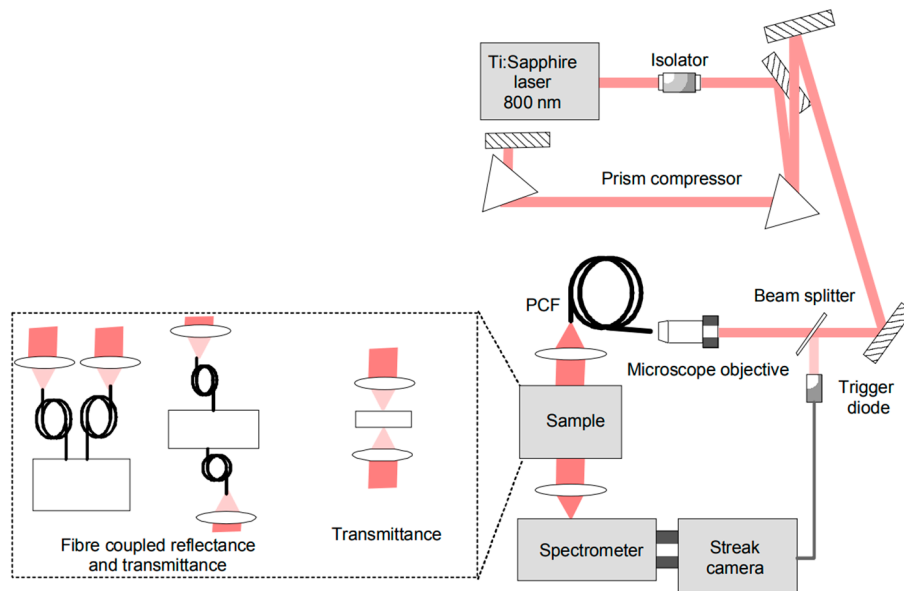


Figure 4. Broadband time domain system based on supercontinuum generation and parallel streak-camera based detection developed by Lund University [60].

A different concept was based on mode-locked lasers, which were sequentially tuned and permitted the use of single-channel TCSPC detection [57], as shown in Figure 5 [22]. As sources, two tunable mode-locked lasers were used, namely, a synchronously pumped dye laser in the 610–700 nm range and an actively mode-locked Ti:Sapphire laser in the 700–1050 nm range. For detection, a microchannel plate photomultiplier (MCP) with S1 surface (R1564U, Hamamatsu, Japan) was used, followed by a chain for TCSPC (SPC130, Becker & Hickl, Germany). The key complexity of this system resided in the handling of the laser sources. Both of them were tunable lasers whose spectral scanning required delicate alignment to provide optimal lasing over the entire range but also automatic control—operated via mechanical actuators—for rotating the intracavity Lyot’s filters. In addition, the Ti:Sapphire laser demanded automatic switching of the output mirror to avoid spurious laser emission as well as a fine adjustment of the cavity length to compensate for chromatic dispersion. A replica of the instrument response function (IRF) was implemented to compensate for variations in pulse shape and detector response during the wavelength tuning and to provide real-time feedback for automatic optimization of the cavity length. This reference IRF was achieved by splitting a small portion of the laser that was directly fed to the MCP. Despite the inherent complexity of the system, the fully automated operation was achieved, permitting the first acquisition of *in vivo* absorption and scattering spectra of various biological tissues by time domain diffuse optics over a wide spectral range (600–1000 nm) [61]. Surely, the adoption of TCSPC permitted to reach high sensitivity and dynamic range, and cover the critical region of high water absorption (above 900 nm), where signal attenuation is dramatically increased as compared to the 700–800 nm range.

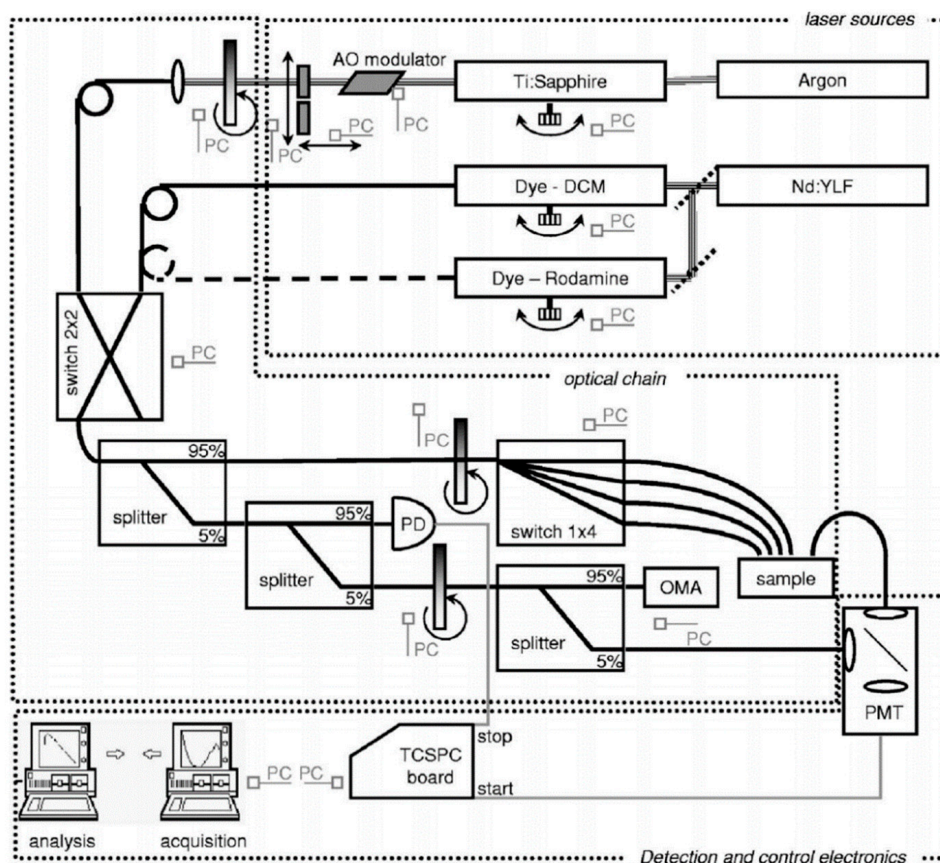


Figure 5. Broadband time domain system based on sequential tuning of mode-locked lasers and time-correlated single photon counting developed by Politecnico di Milano [22].

The introduction of compact commercial supercontinuum sources based on fiber amplified lasers coupled to photonic crystal fibers [62–64] and of rugged silicon photomultipliers [65] usable in diffuse optics [43,66] made it possible to realize movable rack-based systems suitable for use in clinical settings, as shown in Figure 6 [23,67]. Automatic wavelength selection of the supercontinuum source (SC450, Fianium, UK) was achieved by dispersing the light using a rotating prism and selecting a narrow band with a slit. The system was mounted on a cart and permitted non-invasive clinical studies on the application of broadband diffuse optics to bone tissues [29] and thyroid [68].

The implementation of a TCSPC detection scheme—granting single-photon sensitivity, but operated in a parallel configuration—required the use of multianode detectors and multichannel TCSPC boards. A realization is shown in Figure 7 [69]. The source was a supercontinuum generated in a photonic crystal fiber (NL-2.4-800, Blaze Photonics, UK) by a self-locking mode-locked Ti:Sapphire oscillator (Tissa 50, CDP Systems Corp., Russian Federation). Diffusely re-emitted light was dispersed by an imaging spectrometer (SP-2150, Acton Research, USA) and detected by a 16-channel multianode PMT (R5900U-01-L16, Hamamatsu, Japan) connected to a TCSPC board (SPC-630, Becker & Hickl, Germany). Routing bits, associated with the PMT channels hit by the impinging photons were processed by the TCSPC router electronics (PML-16, Becker & Hickl, Germany) to separate signals arising from different wavelengths. This configuration enabled the fully parallel acquisition and permitted to track dynamic variations in absorption and scattering spectra following hemodynamic changes. The key constraints were a limited spectral range (520–850 nm) imposed by the available multichannel PMTs as well as reduced dynamics due to the need to accommodate all wavelengths with different signal attenuation in the same acquisition.

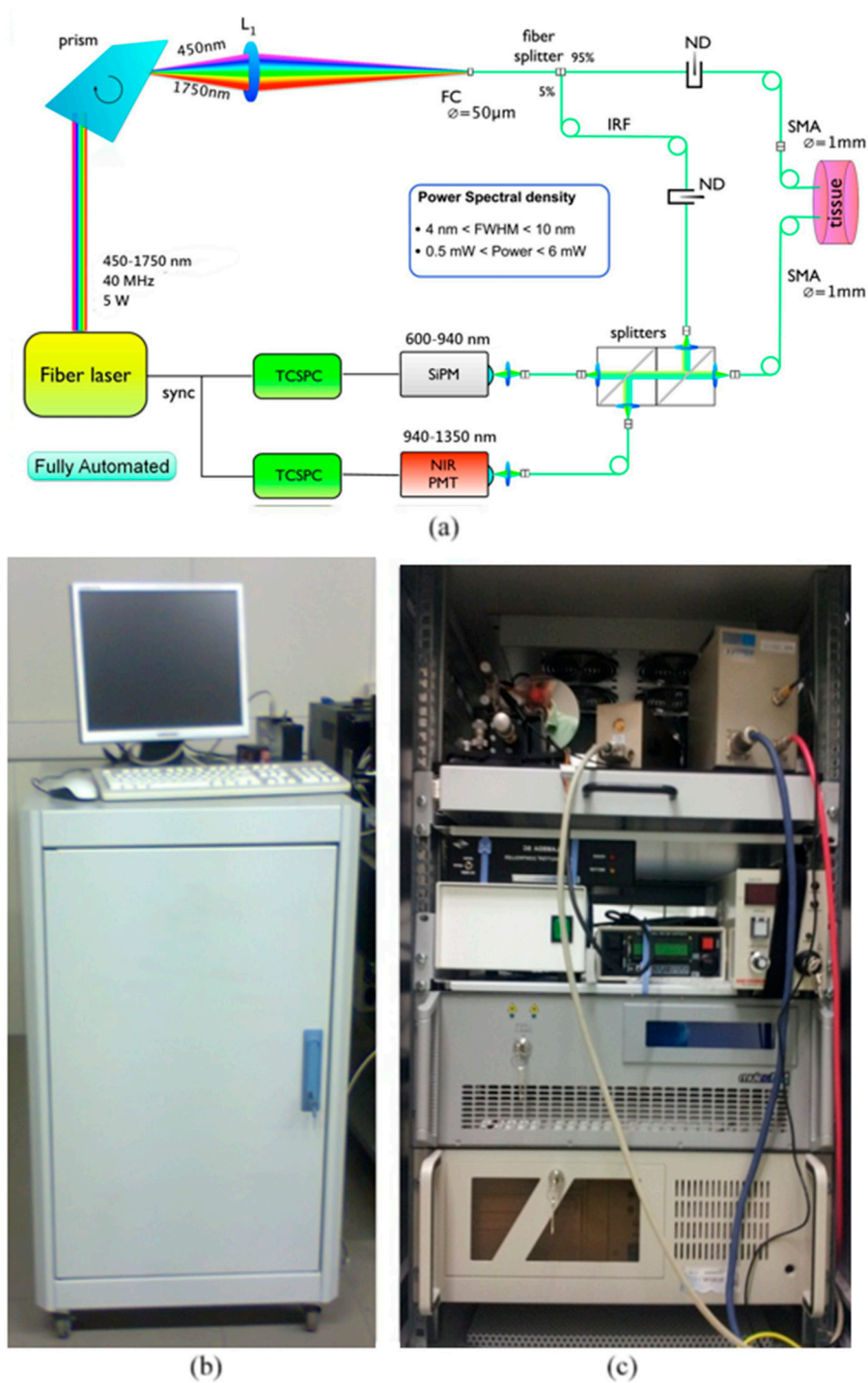


Figure 6. Portable broadband TD-DOS system compatible for clinical use: (a) System optical layout (b) Picture of the portable system on wheels ($111 \times 81 \times 61 \text{ cm}^3$); (c) Internal view of the system with optical chain arrangement on top and detector console, supercontinuum laser in the middle [23].

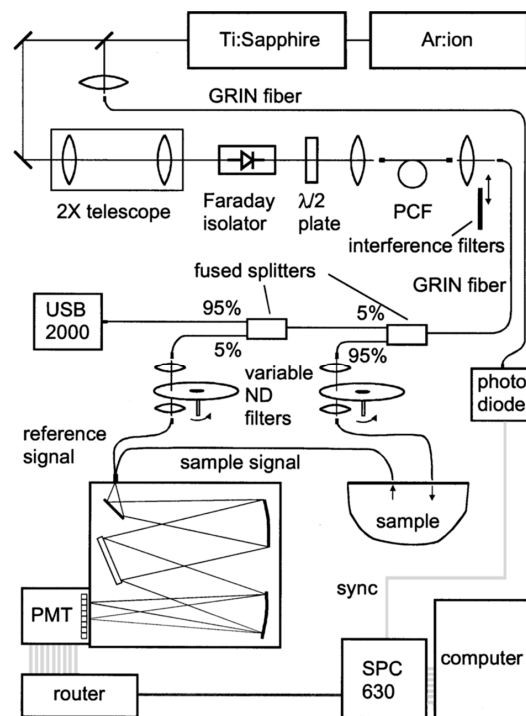


Figure 7. Parallel single photon counting broadband system based on a supercontinuum source and a multianode detector coupled to a multichannel time-correlated single-photon counting (TCSPC) board [69].

Using a similar scheme and a compact detection stage with an integrated spectrometer and multichannel detection (PML Spec, Becker & Hickl, Germany), it was possible to construct a clinically compatible parallel broadband diffuse optical spectrometer as shown in Figure 8 [70]. The parallel acquisition permitted to follow the in vivo dynamics of Indocyanine Green, a contrast agent approved for clinical use, which is used for tracking blood content, as well as extravasation in leaking vasculature as for brain injury [71–75] or tumors [76,77]. As a pilot study, the disentanglement of intracerebral from extracerebral absorption changes on phantoms and healthy volunteers was demonstrated [70].

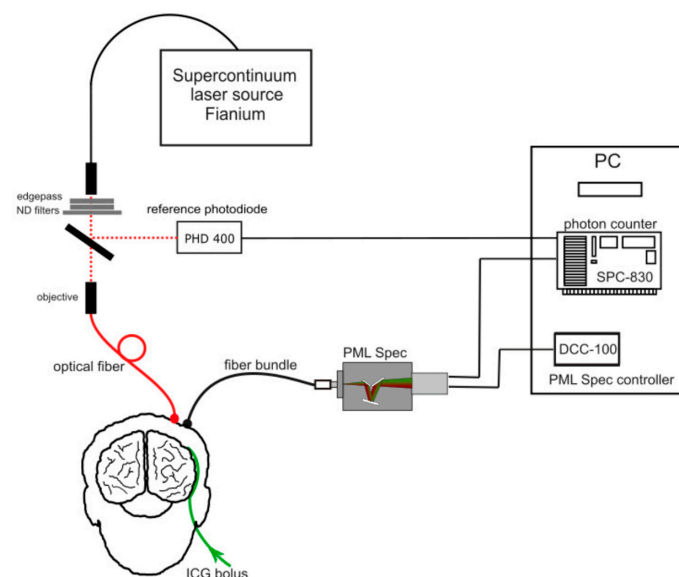


Figure 8. Multiwavelength parallel system developed by Nalecz Institute of Biocybernetics and Biomedical Engineering, Polish Academy of Sciences [70].

4. Analysis

A variety of approaches have been applied for solving and approximating the solution of the RTE. These can be divided into three main categories: i) Analytical, ii) Numerical, iii) Stochastic solutions. The recent advancements in these categories fostered by the power given by parallel computing (graphical processing unit (GPU), multicore, cluster, etc.) allow the solution of the RTE in almost every geometry in reasonable computation time. Hereafter, a resume of these methods is presented.

4.1. Analytical Models

One of the first approximations derived from the RTE is the diffusion equation (DE) [78]. Starting from the RTE, the radiance, the source, and the phase function are decomposed into a spherical harmonic series. Depending on the number N of terms retained in the calculus, the approximation is called PN. As an example, for P1, the functions are approximated as the sum of isotropic and a slightly anisotropic term:

$$\begin{cases} L(\mathbf{r}, \mathbf{s}, t) \simeq \frac{1}{4\pi} \Phi(\mathbf{r}, t) + \frac{3}{4\pi} J(\mathbf{r}, t) \cdot \mathbf{s} \\ Q(\mathbf{r}, \mathbf{s}, t) \simeq \frac{1}{4\pi} Q_0(\mathbf{r}, t) + \frac{3}{4\pi} Q_1(\mathbf{r}, t) \cdot \mathbf{s} \\ p(\mathbf{s}, \mathbf{s}') \simeq \frac{1}{4\pi} + \frac{3}{4\pi} g(\mathbf{s} \cdot \mathbf{s}') \end{cases} \quad (2)$$

where g is the anisotropy factor, defined as the average value of $(\mathbf{s} \cdot \mathbf{s}')$, which is the cosine of the scattering angle. This approximation, in turns, brings to a coupled equation between $\Phi(\mathbf{r}, t)$ (the fluence) and $J(\mathbf{r}, t)$ (the flux), whose solution allows one to derive the radiance, which in turn help the derivation of the signal transmitted or reflected. Solutions to the P3 approximation have been recently derived in a semi-infinite medium [79].

Moreover, by introducing the approximations of (i) $\mu_a \ll \mu'_s = \mu_s(1 - g)$, (ii) an isotropic source term, and (iii) a smooth temporal variation of $J(\mathbf{r}, \mathbf{s}, t)$, Equation (2) becomes:

$$\begin{cases} \left(\frac{1}{v} \frac{\partial}{\partial t} - \nabla \cdot D \nabla + \mu_a \right) \Phi = Q_0 \\ J = -D \nabla \Phi \end{cases}, \quad (3)$$

where $D = \frac{1}{3\mu'_s}$ is the diffusion coefficient. The first Equation of (3) is the well-known diffusion equation (DE) and, together with the Fick's Law (second Equation (3)), has been widely used for analytically solving diffusion problems in a variety of geometries, such as: layered laterally infinite media, layered cylinder, sphere, parallelepiped [80–85]. The diffusion approximation was shown to work quite well in situations in which the diffusion is higher than the absorption and where the source-detector distance allows the detection of photons having undergone a number of scattering events such that the radiance L becomes almost isotropic [86]. Furthermore, the RTE equation has been recently solved in the time domain for a layered medium by Liemert et al. [80], showing a perfect agreement with Monte Carlo simulations, which is considered the gold-standard for model testing.

4.2. Numerical Models

When the complexity of the tissue to model is high, either because of a heterogeneous distribution of optical properties inside or because of the complex shape (e.g., mouse, hand, finger, brain) or both, no explicit solutions can be found to the RTE or to the DE. In this case, the typical approach consists in the numerical calculation of the solution using a finite-element approach (FEM), which is well suited for the DE [87,88]. To get the time domain solution, the typical approach is to apply the FEM to the spatial coordinates and a finite-difference scheme for the evolution in time.

The advantage of this approach is that, once the optical properties of the medium have been defined in the mesh, the solution relies on solving a series of sparse linear systems with the same matrix, which can be efficiently implemented on GPUs [88]. At each temporal step, the fluence distribution in the medium is computed for each source, subsequently, a projection operator (which does not change with time) is used to compute the signal on the detectors. The computation time depends on the

fineness of the mesh, which in turn affects the matrix dimensions, and on the number of light sources. The number of detectors does not affect the computational time because it is a simple projection operation once the fluence is determined.

To further speed up the finite-difference scheme, which is the main bottleneck of this approach, a superposition of solutions obtained in the temporal frequency domain has been recently proposed [89].

4.3. Stochastic Models

Another approach, which unifies both the accuracy of the RTE and the flexibility of modeling a complex tissue, is based on Monte Carlo (MC) simulations. Provided the distribution of optical properties, the phase function, and the boundary conditions, the photon propagation is managed in a stochastic way. Basically, a probability distribution is generated for the occurrence of both the scattering and absorption events in the medium, whilst the phase function is used for sampling the direction at every scattering event [78,90]. A variety of techniques can be implemented for reducing the variance of an MC simulation. A comparison of the different approaches can be found in [91].

An interesting advantage of MC in time domain is the possibility of generating all the combinations of absorptions by using only one simulation with fixed scattering. This requires one to save, for each detected photon, its pathlength in every region of the sample. Once this data is stored, the absorption is introduced by weighting the photon contribution with the formula shown in Equation (4):

$$w = \sum_{i=1}^N \exp(-\ell_i \mu_{ai}), \quad (4)$$

where ℓ_i is the pathlength of the photon inside the region i out of the N regions.

The MC computation is well suited for taking advantage of massively parallel computation. In fact, each photon is independent of the others and, using a parallel approach, a multitude of photons can be launched in parallel [92–97]. The introduction of GPUs has dramatically accelerated the computation time of MC simulations, paving the way to the possibility of using them as a forward model in inverse problems [97,98].

4.4. Perturbative Approaches

A typical case-of-study in TD-DOS is the localization and characterization of a small localized perturbation of the optical properties over an otherwise homogeneous background tissue. This can be representative, as an example, of a lesion in the breast, activation in the brain, etc. Moreover, in diffuse optical tomography (DOT), which consists in the 3D reconstruction of the optical properties by means of measurements on the boundary of the tissue, a key issue is the knowledge of the sensitivity of each measurement for a given localized change of optical properties [99,100], which in turn is the signal variation due to a small localized perturbation in every internal point of the sample.

The most common approach to the perturbative problem relies on the expansion of the fluence $\Phi(\mathbf{r}, t)$ as:

$$\Phi = \Phi_0 + \delta\Phi, \quad (5)$$

where Φ_0 is the unperturbed fluence, and $\delta\Phi = \delta\Phi_{abs} + \delta\Phi_{sca}$ is the perturbation to the fluence due to a variation of absorption and scattering. Equation (5) leads to a DE for $\delta\Phi$ involving the locally perturbed optical properties $\delta\mu_a$ and $\delta\mu_s$. If $|\delta\Phi| \ll \Phi_0$, the resulting approximation is named Born approximation, under whom analytical expressions can be computed in simple geometries, such as layered slab, cylinder, sphere, and parallelepiped. Nevertheless, more accurate solutions can be even found iteratively [101].

If the perturbation is strong, the Born approximation is weak, and other strategies were proposed based on higher order approximation [102–105].

Exploiting MC methods, Sassaroli et al. [106,107] introduced a fast method for computing the perturbed fluence, which is based on: (i) the storage of the pathlength of each photon both in the background medium and in the perturbation volume, and (ii) the storage of the number of scattering interactions inside the perturbation volume [106,108]. This method is based on one single simulation and a re-weighting rule for each trajectory based on the aforementioned information. The approach is exact, but the result is strongly limited by the noise of the MC simulation. Finally, an approach based on the angular decomposition of the radiance derived by MC for retrieving the sensitivity map for both absorption and scattering was proposed [47].

4.5. Multivariate Approach

The temporal curves can also be analyzed by considering multivariate tools. In their simple formulation, the above mentioned methods do not take the spectral dimension of the data into account: they evaluate each wavelength separately. A procedure involving multivariate methods could be used to process TD-DOS data across the entire wavelength range. MADSTRESS is a multivariate tool based on linear regression and on a two-dimensional (2D) interpolation procedure. This method was used to calculate the absorption and scattering coefficients of apples and fructose powder [109,110].

4.6. Final Considerations

As mentioned at the beginning of the section, nowadays the computational power has strongly accelerated the possibility to use almost all methods to solve an inverse problem, ranging from a simple homogeneous medium to a 3D tomography. The DE can be easily overcome by MC, RTE, PN solutions.

TD-DOS aims at the determination of the optical properties of homogeneous or layered tissues (e.g., brain tissue, muscle, breast, etc.) in a wide range of wavelengths. From this, by using the Beer-Lambert law and a semi-empirical scattering power law [29,111,112], it is possible to retrieve the chromophore concentrations and structural information (see Section 5.2).

To make the analysis more robust, spectrally-constrained approaches were proposed, in which all the DTOFs collected from tissue at different wavelengths were analyzed as a whole with the constrain given by the optical properties of the expected constituents (e.g., water, lipid, collagen, hemoglobin) [113,114].

When the shape of the sample is complex or the accuracy of MC is needed, it is possible to generate a look-up table (LUT) of simulations and apply the inverse problem by searching and/or interpolating results in the LUT [115,116]. This avoids the repetitive computation of MC, which, however, nowadays efficient, could not reach the computation speed of an analytical formula.

Finally, an advanced fitting method was proposed to be used when there is an a priori knowledge of the probability distribution of the unknowns (typically absorption and scattering) or uncertainties in the experimental measurement (e.g., uncertainty on the temporal calibration). It is possible to include these uncertainties in the analysis process using a Bayesian approach and thus improve the estimation of the optical properties [117,118].

5. Applications

5.1. Characterization of Absorbers/Tissue Constituents

Absorption spectra of various absorbers are essential for the quantitative analysis of highly scattering media. In tissue optics, the characterization of highly scattering tissue constituents like collagen, elastin, lipid, thyroglobulin using traditional spectrophotometers pose several challenges [119]. An integration sphere could uncouple the effects of scattering, but falls short to address uncoupling from other effects like fluorescence, finite boundary effects, physical structure of tissue constituents, and so on. TD-DOS can be used to characterize highly scattering absorbers [120,121]. By careful design of the measurement protocol, TD-DOS can effectively address the above-mentioned challenges to extract the absolute absorption spectra of various absorbers [119].

Collagen is a structural protein and an abundant tissue constituent present in various soft and hard tissues. Recent works have shown the correlation of collagen density with breast cancer [122,123], other studies aimed at the non-invasive characterization of collagen in bone [26,52]. The first time domain characterization of collagen tissue was presented by Taroni et al. over the range of 600–1100 nm [124,125]. Konugolu Venkata Sekar et al. extended this range to 500–1700 nm by addressing challenges related to fluorescence contamination and decrease in reduced scattering beyond 1100 nm [121]. Figure 9 shows the broadband collagen spectrum with its characteristic peaks around 910, 1030, 1200, and 1500 nm. This opens up the opportunity to explore collagen content in shortwave near infrared (SWIR) range, which has great potential for penetration depth due to low tissue scattering.

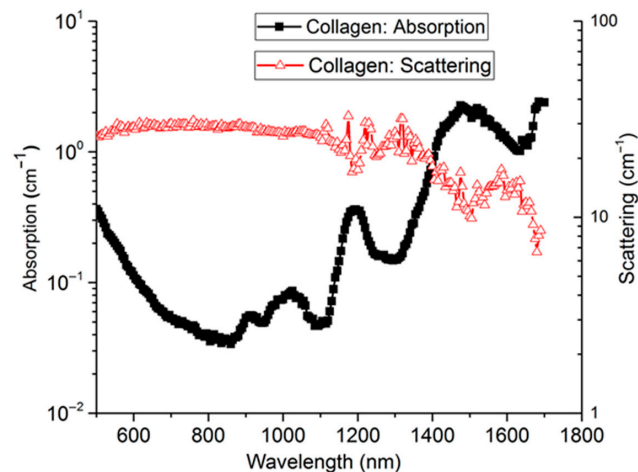


Figure 9. Absorption (black solid squares) and reduced scattering (red triangles) spectra of Type I collagen (bovine Achilles tendon) [122].

Elastin is a protein responsible for the elasticity in the tissues such as skin arteries, ligaments, and lungs. The ratio of elastin to collagen content is a cursor for dermal skin aging [126] and reduced elasticity of the tissue was correlated to breast cancer [127,128]. Figure 10 shows the broadband elastin spectrum measured using elastin extracted from bovine neck ligament [129]. The key features of the elastin spectrum are peaks at 910, 1025, 1185, and 1275 nm. Elastin has similar spectral features to collagen, thus making it difficult to uncouple the two constituents in human tissue, where they often coexist. However, the peak at 1275 nm (and the relative weight of other peaks) could be used to distinguish elastin from collagen, as shown by a close comparison of the two absorption spectra [129].

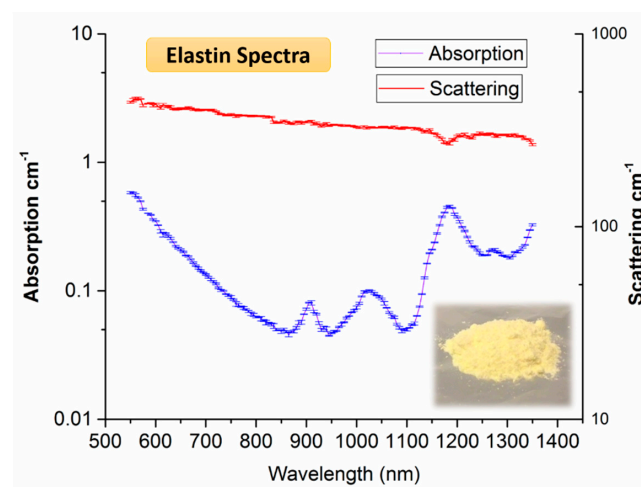


Figure 10. Absorption (blue) and reduced scattering (red) spectra of elastin with standard deviation error bars. The visual appearance of elastin powder is also shown on the bottom right [129].

Lipids play a crucial role in the onset and progression of various fat-related diseases like obesity, metabolic disorder, lifestyle-related morbidity [130,131]. Hence, the optical characterization of lipids could enable their non-invasive quantification for in vivo studies with various diagnostic aims. The time domain broadband (600–1100 nm) diffuse optical characterization of lipid was initially performed on purified pork fat, as reported in Figure 10a [125]. The extension of the characterization to the SWIR window is shown in Figure 11b, where the spectrum measured using TD-DOS [132] is overlaid on the one obtained with CW DOS performed at a small source-detector distance on beef fat. Combining the results in the two spectral ranges, one could obtain a broadband spectrum across the 600–1700 nm range. In the NIR range, an intense and sharp 930 nm peak is unique to lipid. Features of lipids in the SWIR range slightly overlap with the collagen spectrum. However, on careful notice, the lipid peak at 1400 nm is less intense and red-shifted as compared to the collagen peak.

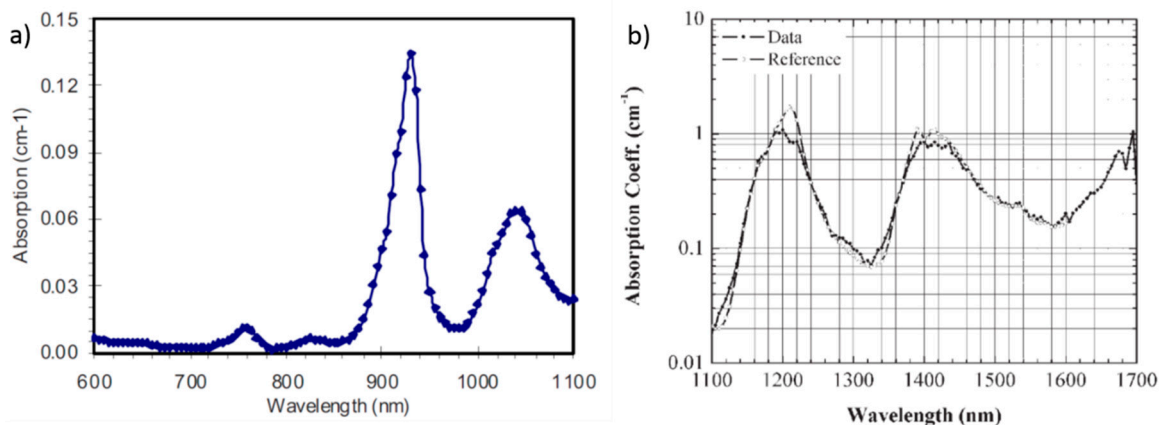


Figure 11. Absorption spectrum of lipid (pork fat): (a) in the near infrared (NIR) [125] and (b) in the shortwave near infrared (SWIR) [132].

Recent studies on the near infrared (NIR) characterization of human thyroid in vivo revealed some unique features [53,68,133]. The quantification of tissue constituents using typical chromophores (lipid, water, collagen, oxy, and de-oxy hemoglobin) resulted in an overestimation of some tissue constituents. This led to the hypothesis of missing constituents that are unique to thyroid tissue. Figure 12 shows the characterization of thyroid-specific tissue constituents: thyroglobulin, tyrosine, and iodine [119]. Thyroglobulin, the most abundant protein in thyroid tissue, has a monotonous decreasing absorption spectrum with a shoulder and a peak, respectively, at 1000 and 1190 nm. Multiple features are found in the tyrosine spectrum with 6 peaks (875, 915, 1090, 1145, 1185, 1290 nm) spread across the broadband 600–1350 nm range. Iodine was found to have an exponential decaying absorption spectrum with minimum to no absorption at long NIR wavelengths. The inset in Figure 12 describes the anatomy of the human thyroid and the breakdown of tissue constituents. Though the potential of the in vivo characterization of the thyroid so far has only been limitedly explored, a few examples are presented in the next section.

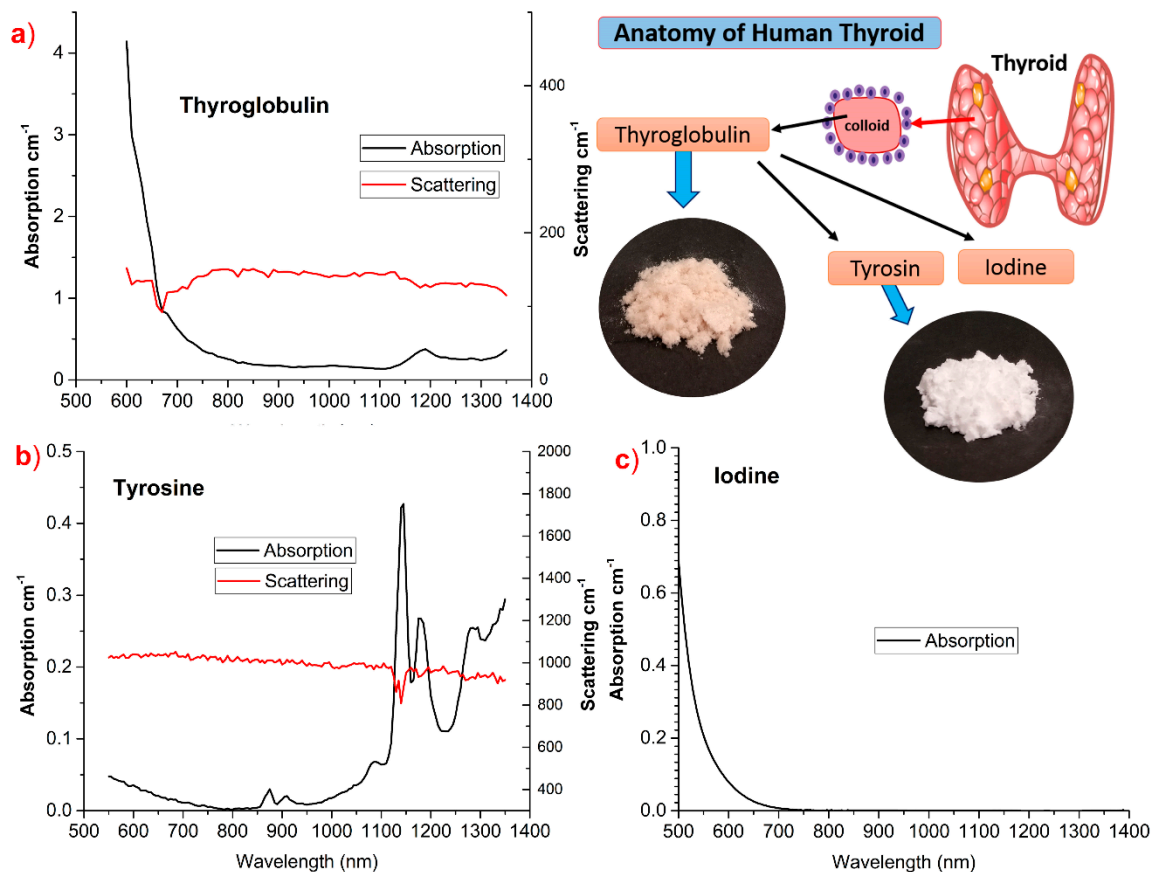


Figure 12. Absorption (black line) and reduced scattering (red line) spectra of thyroid tissue chromophores: (a) thyroglobulin, (b) tyrosine, (c) iodine, with inset depicting the anatomy of thyroid [119].

5.2. In Vivo Characterization of Biological Tissues

TD-DOS combines distinctive features, such as non-invasiveness, deep tissue penetration, and capacity to provide functional information, which makes it a potentially powerful means for the characterization of biological tissues *in vivo* either for physiology studies or for clinical diagnostics.

Since the initial developments of DOS, researchers have shown interest in breast cancer-related applications. They include diagnosis (detection and discrimination between malignant and benign breast lesions), as well as therapy monitoring and cancer risk assessment. Each of these goals can take advantage of a thorough optical characterization of breast tissue, as can be achieved through broadband TD-DOS spectroscopy.

Breast tissue is inherently heterogeneous with two major components: fibro-glandular and adipose tissue. Inter-subject variability is very strong, spanning from fully adipose (BI-RADS category 1) to extremely dense breasts (BI-RADS category 4), where BI-RADS category is the clinical metrics to quantify “breast density”, that is the fraction of radio-opaque fibro-glandular tissue in the breast, based on visual inspection of X-ray mammographic images [125].

Figure 13a shows typical examples of absorption spectra obtained *in vivo* from breasts of different types (i.e., composition), performing TD-DOS measurements in transmittance geometry, and interpreting the data with the solution of the diffusion equation for a homogeneous slab model. Notwithstanding the simple modeling, which is most often used to interpret breast data, the measured absorption properties are really sensitive to tissue composition. At short wavelengths, the major features are always the trailing edge of hemoglobin absorption, increasing upon decreasing wavelength, and the minor peak of deoxygenated hemoglobin (deoxyHb) around 760 nm. Instead, strong variability

is observed above 900 nm, as a result of different tissue composition. The spectrum of the adipose breast (red symbols) is dominated by the absorption peaks of lipids around 930 and 1040 nm, while the highly fibro-glandular breast (blue symbols) is characterized by very strong water absorption around 980 nm, with collagen weakly contributing as a shoulder on the trailing edge of the water peak.

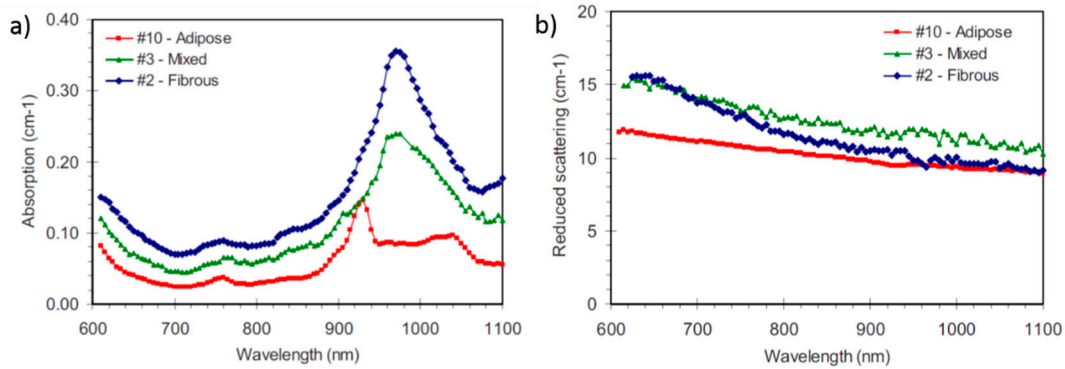


Figure 13. (a) Absorption and (b) reduced scattering spectra measured in vivo from breasts of different types, highlighting the marked inter-subject variability of this tissue [125].

Interpreting the absorption spectra with the Beer law enables the estimate of tissue composition: oxy- and deoxyhemoglobin, water lipid, and collagen (or a subset) are thus quantified. From the two forms of hemoglobin, more commonly used physiological parameters are then derived: total hemoglobin content (tHb) and oxygenation level (SO₂).

Figure 13b reports the reduced scattering spectra measured from the same three subjects. The spectrum of the dense (fibrous) breast typically shows a steeper slope than that of adipose or mixed breasts. That reflects the different composition: lower lipid and higher collagen content. Actually, the reduced scattering spectrum is generally interpreted with a simple empirical approximation to Mie theory [112,113] and provides information on the microscopic structure of tissue: $\mu_s' = a\lambda^{-b}$, where the amplitude a is related to the number of scattering centers (cell membranes, subcellular organelles, etc.) and the slope b depends on their size, being higher for smaller scattering centers.

Table 1 displays the results obtained interpreting the absorption and reduced scattering spectra shown in Figure 13. Both tissue composition and scattering parameters related to the microscopic tissue structure can vary markedly with breast type.

Table 1. Inter-subject variability of breast tissue composition [125].

Breast Type	Tissue Composition					Scattering Parameters	
	tHb (μM)	SO ₂ (%)	Lipid (mg/cm ³)	Water (mg/cm ³)	Collagen (mg/cm ³)	a (cm ⁻¹)	b
Adipose	10.0 ± 1.2	71 ± 10	737 ± 52	111 ± 15	24 ± 5	13.4 ± 2.0	0.69 ± 0.28
Mixed	24.1 ± 2.0	84 ± 1	428 ± 24	302 ± 80	60 ± 1	16.1 ± 0.5	0.71 ± 0.03
Fibrous	24.3 ± 1.8	80 ± 1	173 ± 56	615 ± 40	107 ± 22	17.6 ± 1.1	1.16 ± 0.09

Clinical applications often impose limitations on overall measurement time. Thus, it is important to determine whether tissue quantification can be achieved even operating at a limited number of wavelengths. The scattering spectra can be modeled with just two parameters (a and b), while the absorption should generally provide information on (at least) 5 constituents for thorough tissue characterization. Thus, measurements need to be performed at least at (at least) 7 distinct wavelengths, spread over a broad spectral range, including marked absorption features of all the constituents of interest (i.e., 600 to 800 nm for blood, and including the range of 900 to 1100 nm for water, lipids, and collagen). The acquisition of the full spectrum provides more robust results, but satisfactory outcomes can be obtained even from data collected at a small set of wavelengths (7), provided that

global data fitting with spectral constrains is performed [113]. Actually, using that spectral approach, optically derived tissue parameters were effectively used in the discrimination between malignant and benign breast lesions [13], in the optical measurement of breast density (important risk factor for developing cancer [134]), and in the identification of women at high risk for their high breast density [123].

The knowledge of the optical properties of the human head is quite valuable for the development of non-invasive optical technologies that aim at imaging or monitoring brain functions or injuries. Understanding the biological variability in the optical properties of head layers (scalp-skull, gray matter, cerebrospinal fluid, white matter) is beneficial for setting up simulation scenarios, optimizing existing technologies, analyzing actual measurements with a priori information (e.g., on the optical pathlength). Figure 14 shows the results of a multilaboratory exercise where 3 different approaches—namely a multi-distance CW system, a 5-wavelength time-resolved instrument, and a broadband TD-DOS workstation—were challenged in retrieving the optical properties of the forehead of 9 subjects [135]. In particular, the broadband TD-DOS system (blue squares) was the only one apt to cover a wide spectral range (600–1100 nm), thus revealing the clear contribution of lipids and water to tissue absorption. The broadband TD-DOS data were analyzed using a homogeneous solution of the diffusion equation. Simulations highlighted that the spatial region determining the retrieved parameters is the brain for what concerns the absorption, and the skull for the scattering. In the case of the few-wavelength TD-DOS system, exploiting a multi-distance approach and longer time-per-wavelength acquisition, it was also possible to apply a two-layer model, to disentangle the scalp-skull properties (black circles) from the brain properties (gray circles). The feasibility to apply heterogeneous models is certainly of great interest also for broadband spectroscopy, with the aim to describe biological tissues more accurately and with higher informative content. Key challenges are surely the strong light attenuation above 900 nm, which limits, in particular, the availability of long-lived (>1 ns) photons carrying information from deeper structures (brain). Also, fast and accurate models of photon migration are needed to overcome the key limitations of the diffusion approximation when dealing with short (<200 ps) propagation times or thin (<2 mm) layers. In that direction, especially attractive is the proposal of analytical multi-layered models comparable with Monte Carlo in terms of accuracy, but quick enough to be used in multi-parameter inversion procedures [136,137].

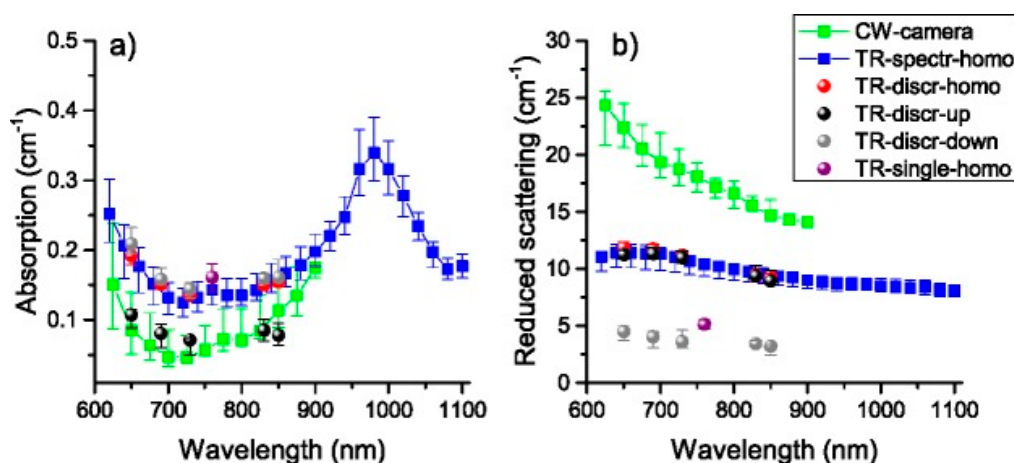


Figure 14. (a) Absorption and (b) reduced scattering spectra of the human forehead. Median values over 9 subjects are shown for data collected with different systems (CW, TD at 5 wavelengths, and broadband TD). A homogeneous model was applied to data from all systems. For the TD system at discrete wavelengths results are displayed also when the data are interpreted with a two-layer model [138].

In the last years, several other TD-DOS applications started to be considered, stemming from presently unmet clinical needs. One of them is the optical characterization of bone. The aging population suffers more and more from bone-related pathologies, but in several widespread cases (e.g., osteoporosis) effective non-invasive means are currently not available for early diagnosis, which instead is key to efficient treatment. An initial attempt towards the non-invasive optical characterization of bone tissue was made more than a decade ago, performing measurements in the 650–1000 nm range on the calcaneus of 7 female volunteers spanning over a broad age range (26–82 y): Measurement feasibility was shown and possible age dependence of the optical properties was suggested to reflect age-related changes in composition and structure of bone tissue [26].

More recently, data were collected from 17 healthy volunteers at 6 locations where the bone is rather superficial and thus accessible to optical probing, with the aim of identifying the best location for further systematic optical studies on bone [29,138]. From Figure 15, it appears that, notwithstanding significant inter-subject variability (measured by the standard deviation), on average different locations are characterized by different optical properties. In particular, lower absorption, with smaller water contribution at 980 nm (calcaneus and trochanter) corresponds to higher scattering.

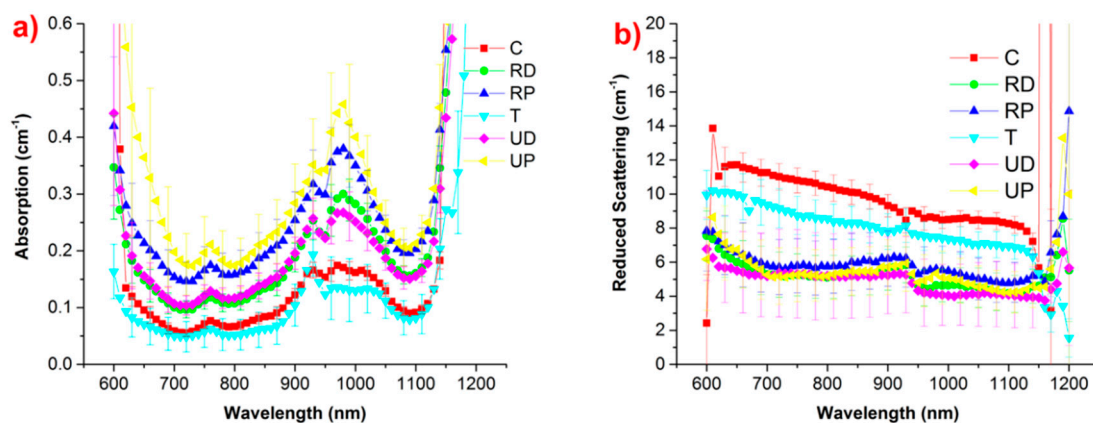


Figure 15. (a) Absorption and (b) reduced scattering properties of bone measured at 6 locations (calcaneus, distal and proximal radius, trochanter, distal and proximal ulna), averaged over 17 volunteers [29].

Looking for an ideal location for clinical diagnostics of bone, three parameters were considered: the thickness of the superficial skin layer, the penetration depth of photons at the wavelength of operation, and the bone volume at the probed location. At the distal radius location, superficial tissue (skin) thickness is small, the high light penetration depth is foreseen based on the measured optical properties, and the bone volume is high, thus providing a strong contribution to the overall collected signal. All in all, these observations suggest the distal radius location as the best one for future diffuse optical studies of bone-related pathologies.

Thyroid nodules are common, but presently their nature cannot be identified non-invasively. Fine needle aspiration followed by cytological analysis is the established standard to diagnose thyroid pathologies. However, besides being an invasive procedure, it may miss up to one-third of malignancies in palpable nodules [139].

A non-invasive optical diagnostics capable to estimate tissue composition and blood parameters may be of real interest. Thus, after the optical characterization of its specific constituents (tyrosine and thyroglobulin), described in Section 5.1, the *in vivo* characterization of the thyroid has recently started [53]. TD-DOS data were collected in reflectance geometry from 6 healthy volunteers on the thyroid area and at a reference lateral position on the neck. At the thyroid location, two source-detector distances d ($d = 1.5$ cm and 2.5 cm) were tested to identify best conditions for probing the gland (as a trade-off between signal level and minimum contribution from surrounding tissues).

These initial measurements reported in Figure 16 show that in the range of 600–1100 nm, the absorption properties at the thyroid location are dominated (around 600 nm) by the tail of hemoglobin and thyroglobulin absorption peaks at shorter wavelengths. Strong water absorption at 980 nm is the other dominant spectral feature. Finally, over the entire spectral range, the absorption is very high, spanning from 0.2 to 1.2 cm^{-1} , which may at least in part be attributed to thyroglobulin. Similar absorption properties are obtained at the two source-detector separations, with just slightly lower absorption below 800 nm for the shorter source-detector distance. In agreement with what expected based on thyroid physiology, the absorption at the reference location is on average lower over the entire spectral range, reflecting lower blood content and no thyroid-specific contributions.

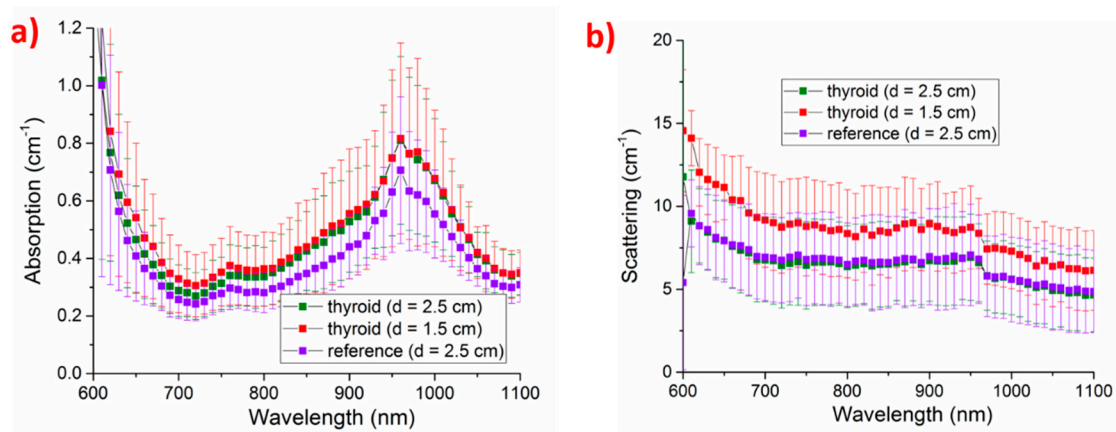


Figure 16. Absorption (a) and reduced scattering (b) properties of thyroid at two source-detector separations d (red squares, $d = 1.5$ cm, green squares, $d = 2.5$ cm), and of a reference lateral location on the neck (violet square, $d = 2.5$ cm) [53].

The measurements on the thyroid with $d = 1.5$ cm resulted in higher reduced scattering than other measurements.

It is important to highlight that just a few subjects were analyzed and that the inter-subject variability is marked. Still, this preliminary study showed that the non-invasive characterization of the thyroid by optical means is feasible and could effectively be further pursued.

Finally, it is interesting to consider adipose tissue. It has long been regarded just as an energy depot, while it is now becoming evident that it is an endocrine organ, deeply involved in the development of many pathologies, like obesity, diabetes, and metabolic diseases that are growing in impact on the quality of life and in burden on the healthcare systems [131,140]. Visceral fat, located mainly within the abdominal cavity has an important link with pathologies. Thus, the non-invasive *in vivo* characterization of abdominal fat and the capacity to monitor its pathologic changes may certainly be of interest for pathophysiology studies.

An interesting work on the optical assessment of abdominal adipose tissue was recently performed with a different approach to diffuse optics (a combination of frequency domain measurements at selected wavelengths and broadband CW measurements interpreted with a homogeneous model of the abdomen). That study suggested that DOS may be of help in monitoring the effects of a low-calorie diet on the obese subjects, and more generally in investigating the role of adipose tissue in metabolic disorders [141].

However, TD-DOS data collected at 610–1010 nm from on the abdomen of 3 healthy volunteers and interpreted with the diffusion approximation for a homogeneous semi-infinite medium showed that, depending on the subject, the absorption spectrum can be dominated by lipid absorption (as expected when the adipose tissue layer is properly probed) or by water and blood, when the subcutaneous adipose tissue is thin and the underlying muscle is reached [142]. That clearly evidenced the need to model the abdomen as a multi-layer structure, when aiming at the quantification of the optical

properties and of the composition of adipose tissue. Further data in support of this need were recently obtained performing TD-DOS on 4 healthy volunteers at 3 different source-detector separations d ($d = 1, 2, 3$ cm), probing increasing depths. As evident from Figure 17, the measured absorption properties markedly depend on depth [143]. With $d = 3$ cm, when the adipose tissue layer is thick (>2 cm), it dominates the estimated absorption properties, which clearly resemble the spectral features of lipid. Instead, for thinner subcutaneous adipose tissue, the absorption properties also depend on water (at 980 nm) and blood (at short wavelengths) of the underlying muscle. On the other end, the contribution of the skin also needs to be considered, as it also shows marked intersubject variability, and possibly age dependence. Thus, a layered model, accounting for skin, adipose tissue layer and underlying muscle, is needed to allow a proper investigation of the adipose tissue.

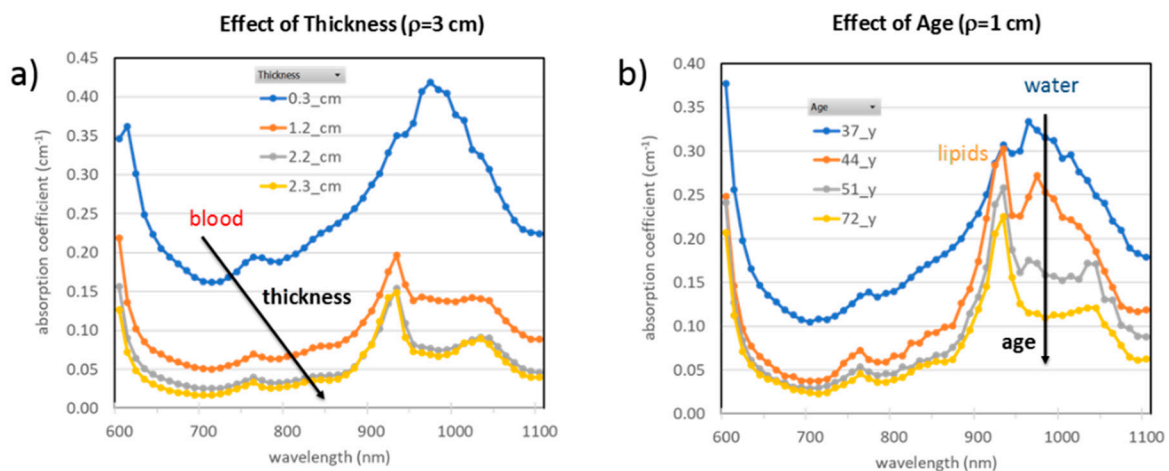


Figure 17. Absorption spectra measured on the abdomen of 4 healthy volunteers with source-detector distance: (a) $\rho = 3$ cm, and (b) $\rho = 1$ cm. The legend shows the thickness of the adipose tissue layer in (a) and the subject age in (b) [143].

5.3. Wood

An interesting field for diffuse optics with potential industrial applications is the non-destructive spectroscopy of wood. This field has been explored at large by different NIR techniques directly focused on non-destructive retrieval of wood composition or conservation status [144–148]. The key advantage of broadband TD-DOS in this field is the intrinsic capability of disentangling absorption from scattering contributions, resulting in a more accurate estimate of the optical properties. An example of an application is the monitoring of archeological wood and in general of age-related degradation of wood artifacts, as shown in Figure 18 [149]. A clear reduction in the scattering coefficient is observed upon wetting—as for waterlogged wood—and even further by artificially procured degradation, due to the decrease of refractive index mismatch among cells and disruption of the cellular structure. The absorption spectra clearly display the water contribution in wet samples (around 980 nm) as well as the increased absorption of oxidative products in the region <800 nm. The strong optical anisotropy of wood materials is evident from the large difference in the scattering coefficient using a source-detector pair parallel (up) or perpendicular (down) with respect to the wood fibers.

The capability to detect water content within the diffusive medium can be exploited for the monitoring of wood moisture—a key parameter with relevance to timber industrial applications [150]. Figure 19 shows a sample specimen kept in a chamber under controlled humidity and continuously monitored using broadband TD-DOS. Upon increasing the humidity level—and therefore the moisture content in wood—the water absorption peak around 980 nm increases correspondingly, demonstrating a sensitivity of the technique down to a few percents of moisture content.

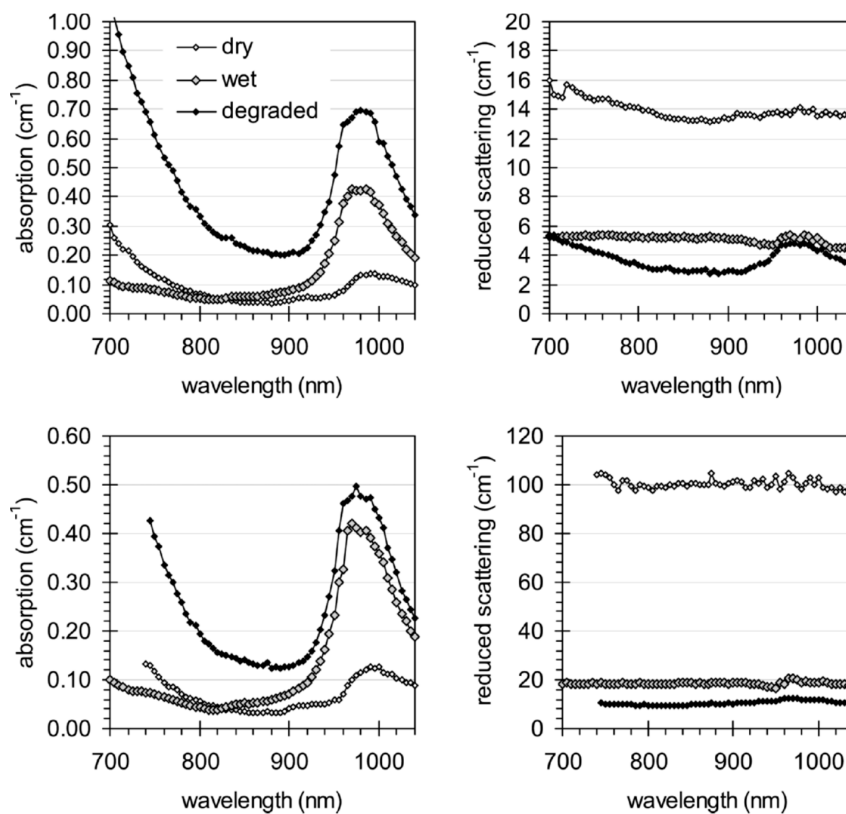


Figure 18. Monitoring the effect of degradation on wood samples measured along the fibers (up), perpendicular to them (down). The scattering spectrum (right) is progressively decreased moving from the dry sample (open diamonds), to wet sample (gray diamonds), and finally to degraded sample (black diamonds). Likewise, the absorption spectrum (left) is increased for the wet sample in the water-absorbing region (around 980 nm) and for the degraded sample in the red region (<800 nm) due to oxidation products. The strong optical anisotropy of wood materials is evident from the large difference in the scattering coefficient in the configuration parallel (up) or perpendicular (down) to the wood fibers [149].

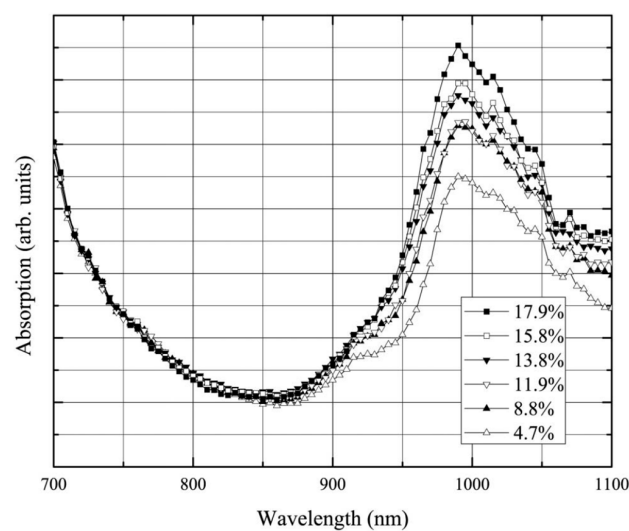


Figure 19. Spectral changes in the absorption spectrum of wood samples under increasing moisture content [150].

A further attractive industrial application was pursued in the quantification of monomer uptake in wood polymer composites [151]. The key interest derives from recent attempts to generate structurally strong wood materials starting from low-quality softwood structures soaked in a (possibly biodegradable) monomer undergoing polymerization. Figure 20a shows the alteration in the absorption spectrum of wood caused by the uptake of a mix of monomers. The wood specimen was immersed in a solution containing the monomer mix (45% glycidyl methacrylate, 45% methylmethacrylate, and 10% ethylene glycol dimethacrylate) and uptake was forced applying mild vacuum to the chamber, while the sample was continuously monitored by broadband TD-DOS. The difference between the treated and untreated wood corresponds to the absorption spectrum of the monomer mix, thus permitting absolute quantitation. Figure 20b demonstrates capabilities to monitor the monomer uptake non-destructively across a 1 cm thick wood sample at different positions on the surface along the specimen with a precision better than 1% [152].

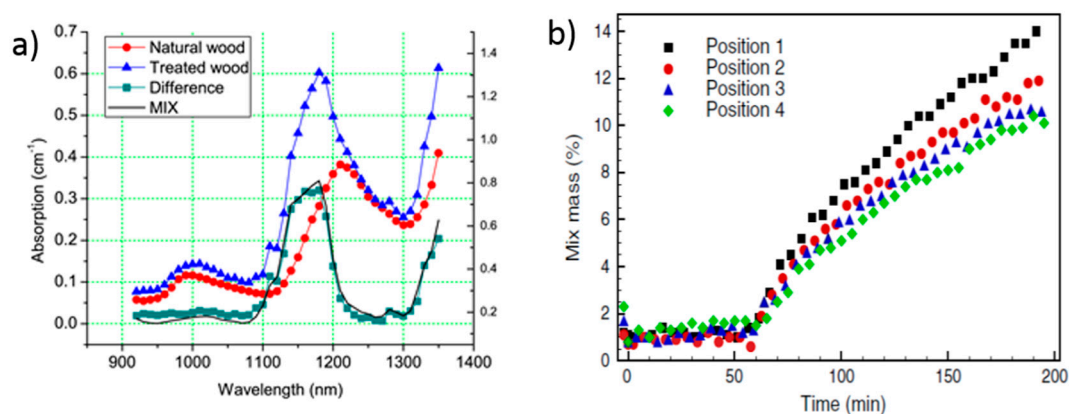


Figure 20. Quantification of monomer uptake in softwood samples. The clear increase in the absorption spectrum (a) of the natural wood around 1100–1200 nm following soaking in the monomer bath (treated wood) is clearly reflecting the absorption spectrum of the monomers (MIX) [151]. The concentration of the monomer at different positions along the wood sample (b) demonstrates a precision in monomer assessment better than 1% in mass [152].

5.4. Food

Besides wood, also food products, and in particular fruits, have been investigated using optical techniques (mainly NIR spectroscopy) [2,153,154], and in particular broadband TD-DOS. Figure 21 displays the absorption and reduced scattering spectra of different fruits and vegetables [155]. The absorption peak of chlorophyll around 670 nm and of water around 980 nm are clearly visible. In the case of kiwifruit, chlorophyll content is so high that only the falling edge of the 670 nm chlorophyll peak is measurable. That initial broadband spectroscopy of food products by TD-DOS permitted to identify the best operating wavelengths for compact off-the-field systems applied to the non-destructive quality assessment of food [156].

Differently from standard NIR spectroscopy, TD-DOS is largely independent of the optical contact or surface pigmentation. Figure 22 clearly shows that the absorption (left) and reduced scattering (right) spectra of different varieties of apples are not affected by skin removal [157]. This property is due to the physics of TD-DOS, since the photon temporal distribution is determined by the combined effect of scattering (creating a spreading of photon paths) and absorption (ruling the survival probability of each random path), as discussed and shown in Section 2. Therefore, thin superficial layers or simply source or contact instabilities will simply change the signal amplitude without affecting the temporal shape, therefore with no impact whatsoever on the retrieved optical properties.

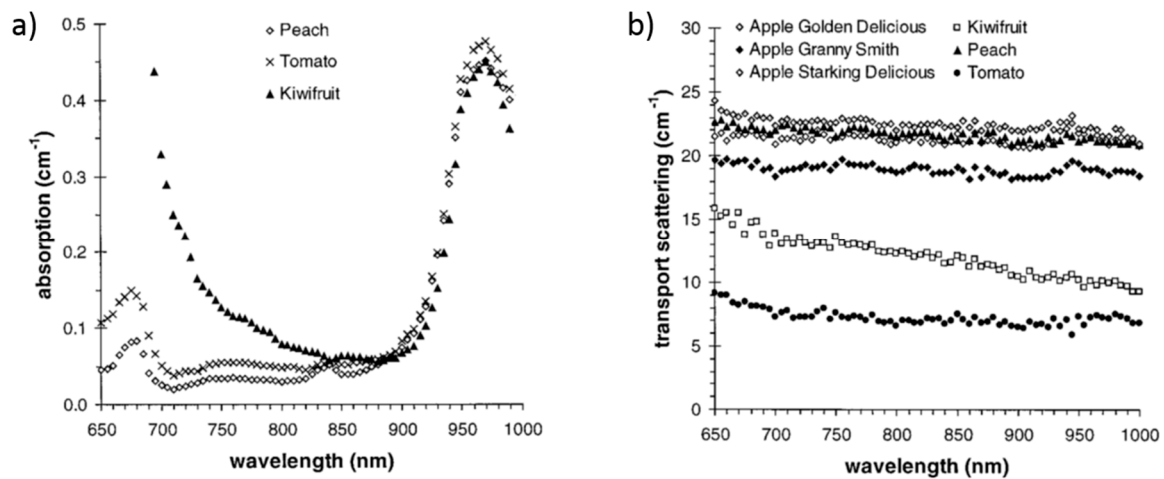


Figure 21. (a) Absorption and (b) reduced scattering spectra of different intact fruits and vegetables [155].

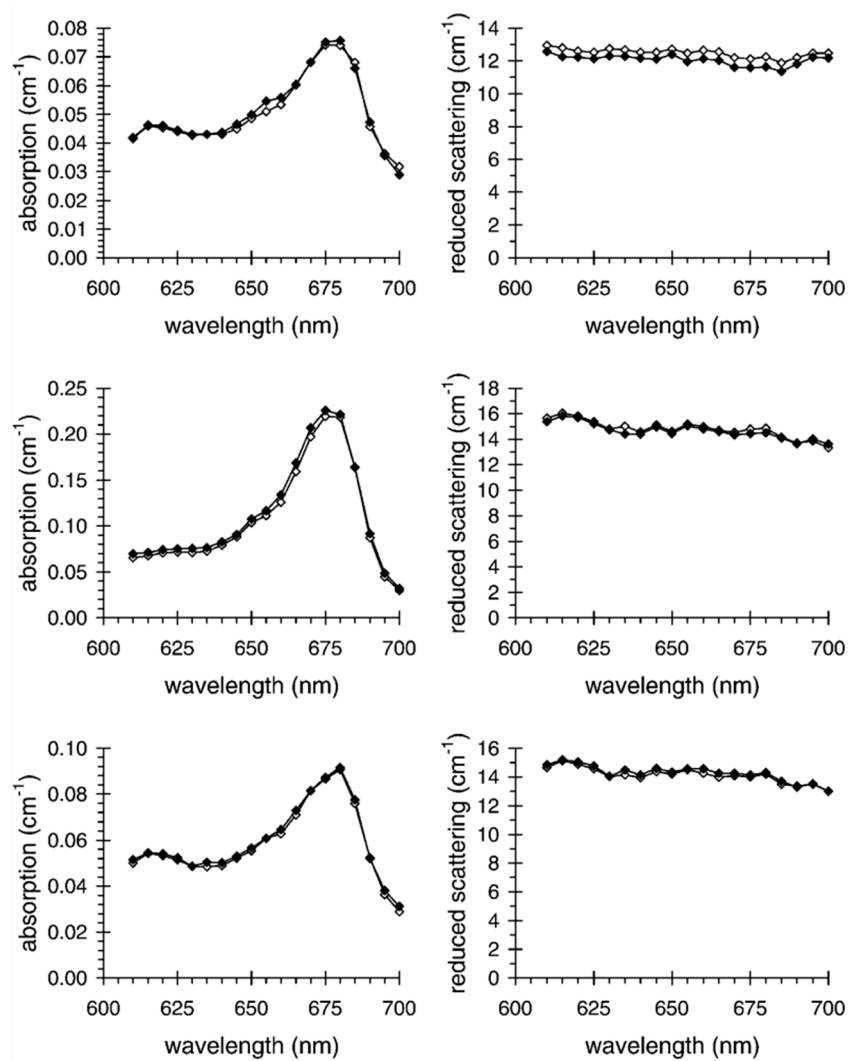


Figure 22. Absorption (left pane) and scattering (right pane) spectra of a Golden Delicious (top row), a Granny Smith (middle row), and a Starking Delicious apple (bottom row) before (filled diamonds), and after (empty diamonds) skin removal [157].

Another field of food quality control and food safety is in the area of dairy products. Several studies have been conducted in this area using photon time-of-flight NIR spectroscopy, enabling independent measurements of the NIR absorption and scattering spectra [158–161].

5.5. Pharmaceuticals

The quality control in the production of pharmaceutical tablets is strict, with tolerances of the amount of active pharmaceutical ingredient (API) of 1%. To secure that the production is providing pharmaceutical tablets with an API content within this narrow interval, typically random tablets are taken out in the production line for wet chemistry analysis. This analysis is time-consuming and labor intense. With results of the analysis available first after a long delay. If the tablet does not fulfill the quality control, it means that large batches of tablets have to be discarded due to the long analysis delay. Direct in-line optical spectroscopic analysis is considered a better technique, provided that the accuracy of the measurements can be sufficiently good. DOS, as well as Raman transmission spectroscopy [162,163], are studied for such analysis. A complication is the highly scattering character of the tablets, providing a very long and spread path of the light as it propagates through a tablet. The scattering is caused by the porous character of the tablet, with changes in the refractive index as light propagates through the tablet. Any alterations in the size distribution of the filling material or the compression force in the production of the tablet will alter the light path as it passes through the tablet. This will cause alterations in measured DOS or Raman spectra, making precise absolute concentration measurements challenging.

The biophotonics team at Lund University had a long-lasting collaboration with AstraZeneca in Molndal, Sweden to assess the potential of near-infrared photon time-of-flight spectroscopy (pTOF or TD-DOS) as a more sophisticated version of near-infrared spectroscopy (NIRS) to allow absorption spectra to be measured independent of the scattering properties of the tablet. Figure 23 shows the extraction of absorption and reduced scattering spectra of tablets with different scattering, showing that the scattering contribution is effectively eliminated by TD-DOS. In this way, the uncertainties caused by variations in scattering properties could be eliminated in the assessment of API concentration, and the scattering properties could be linked to the matrix properties of the tablet, related to releasing properties of the API, including the delay and duration of the release after swallowing the tablet. These measurements could be complemented by NIR gas spectroscopy to further assess the matrix properties of the tablets [64,158,159,162–173].

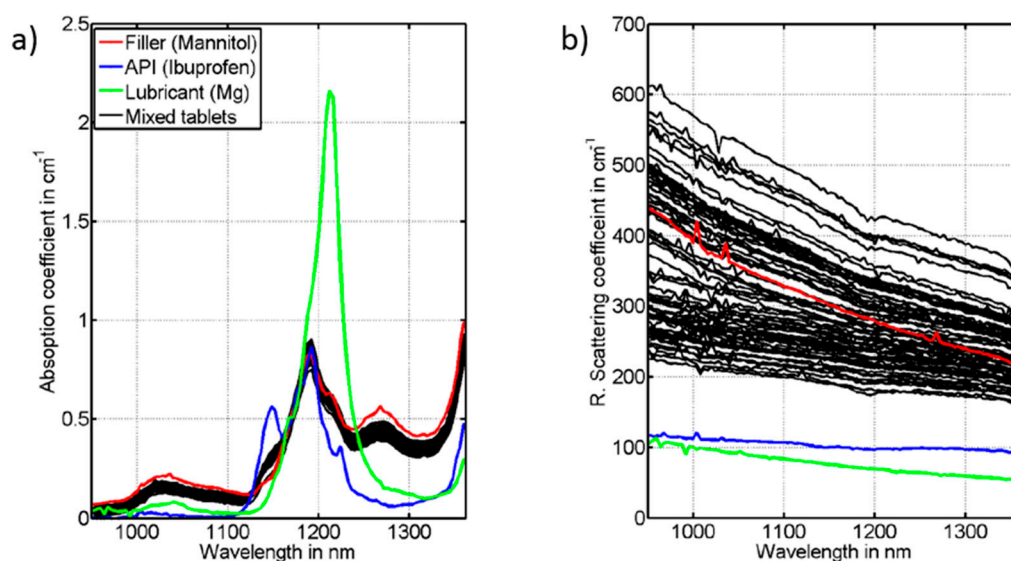


Figure 23. (a) Absorption and (b) reduced scattering spectra of measured tablets (black lines) with different scattering contribution, and of the pure ingredients of tablets (red, blue, green) [161].

5.6. Standardization and Performances Assessment

In the biophotonics field, the need is recognized for shared procedures for performance assessment of newly developed instruments to ensure the reproducibility of results and reliable comparisons between different instruments [170]. Diffuse optics is pursuing this approach [49–51] as it is undergoing great technology progresses, like miniaturization of pulsed laser sources [171], an increase of detector light-harvesting capability [172], high throughput timing electronics [173–175], and innovative measurement technique [176–178]. In the medical imaging field, in particular, it is crucial to enable a solid validation of new or upgraded instruments in laboratory settings, performing measurements on tissue-mimicking phantoms instead of on humans and anticipating possible technical issues that could occur during expensive clinical trials. Consequently, important human and financial investments are being spread, leading to the use of many different materials for the fabrication of phantoms. Phantoms must rely on well-defined recipes, devised thanks to a proper knowledge of the spectral characteristics of the different phantom constituents, and on precise final characterizations to verify their targeted optical properties. Therefore, the role of TD-DOS facilities is crucial. Our purpose here is not to provide an exhaustive review of all the different materials involved in this process, but to make examples where broadband TD-DOS allowed one to solve specific issues.

Ref. [179] presents a phantom kit composed of a homogeneous epoxy resin bulk phantom with a hole, in which different epoxy resin rods can move along one direction (Figure 24a). Each rod contains a different absorption perturbation [180], thus allowing to move the inhomogeneity with respect to the position of the source-detector pair. The kit has been fabricated using titanium dioxide particles to obtain the targeted μ'_s and black toner powder to obtain the desired μ_a . The optical properties of the bulk phantom are shown in Figure 24b. The absorption coefficient is quite flat up to 1100 nm, with a maximum difference in the range of about 0.05 cm^{-1} due to faint absorption peaks proper of epoxy resin. At longer wavelengths, larger absorption peaks of the epoxy resin matrix are clearly visible.

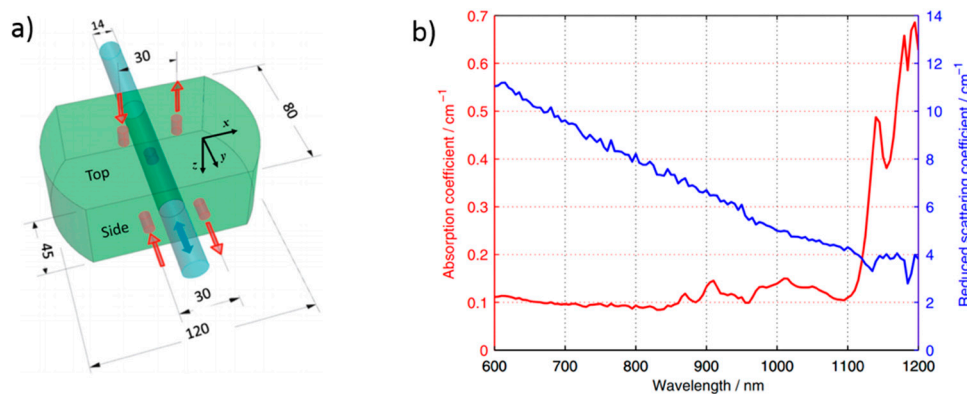


Figure 24. (a) Layout of the switchable phantom with dimensions in millimeters. (b) Absorption and reduced scattering coefficients over a broadband wavelength range [179].

In some cases, even if perishable within a few weeks, the high flexibility of liquid phantoms is required to finely change the optical properties during measurement or to freely move various perturbations. For this reason, phantoms based on water dilutions of Intralipid-20% and India ink have been widely employed. In a multi-center study, the optical properties of these phantoms were characterized in a broad wavelength range (between 633 and 916 nm) [181]. Reference values were identified for the μ_a of India ink and the μ'_s of Intralipid-20%, with uncertainty $<2\%$, providing a solid base for the preparation of liquid phantoms.

Multimodal imaging is emerging as a novel approach to improve the diagnostic performance of a single medical examination by combining the strengths of different measurement techniques. In the field of diffuse optics, there is quite a strong effort in combining, for instance, ultrasound imaging with

diffuse optics [182,183] or different diffuse optics techniques [184]. An example is the combination of DOS and diffuse correlation spectroscopy (DCS) [1]. DCS exploits the autocorrelation function of light speckles intensity, which depends on the speed of moving scattering particles (like red blood cells) to measure tissue microvascular blood flow. Hence, it can provide a complimentary information to DOS. A joint phantom for multimodal optical measurements has to be liquid to allow the proper Brownian motion of the scattering particles. With respect to a standard liquid phantom, in this case, there is also the need to tune the Brownian diffusion coefficient D_b independent of the optical properties. For this reason, the possibility was tested to tune the phantom viscosity by adding glycerol, which has high viscosity and negligible absorption [184]. Unfortunately, its refractive index is very close to that of fat droplets, reducing their scattering power [185]. A TD-DOS system was employed to characterize the μ'_s variation with the relative content of glycerol in water between 600 and 1100 nm (Figure 25b), making it possible to reliably compensate for the decreased scattering power with a calibrated increase of fat droplets concentration, and thus enabling the independent tuning of optical and dynamic properties (Figure 25a).

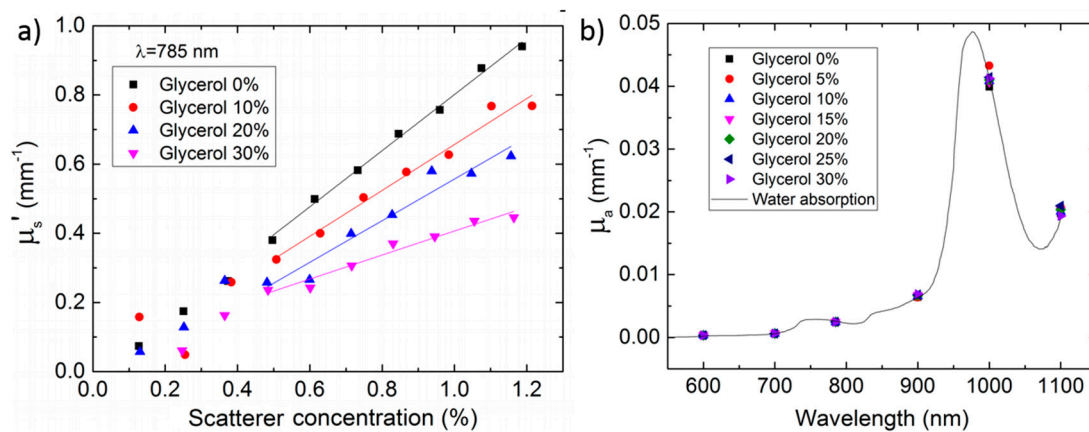


Figure 25. (a) Absorption spectrum of phantoms with different glycerol content. The good overlapping of the measurement points proves the capability to independently tune optical and dynamic properties. (b) Reduced scattering coefficient of glycerol-based phantoms at 785 nm at different concentrations of scattering centers (x axis) and of glycerol content (symbols). The reduced scattering power upon increasing glycerol content is proved by the correspondingly reduced slope of the interpolating lines [184].

To evaluate the performance of a system in retrieving the relative concentrations of different tissue constituents, it is possible to use water-based phantoms with the addition of other chromophores. Water and lipids are major tissue constituents, thus water-based phantoms are the best starting point for mimicking the absorption spectrum of tissues. In this case, lipid dilutions must be replaced with a more realistic fat, like the purified pork fat. Being water and lipid immiscible, different recipes have been developed, based on the simple emulsion of the two using a professional homogenizer (nature emulsion), or with the addition of a thickener, like Agar or Triton-X [186]. The optical properties of these phantoms were characterized on a broad spectral range (600–1100 nm), as shown in Figure 26 for phantoms containing Triton-X. This allowed one to identify the range of tissue optical properties that can be covered in the 3 cases. While nature emulsions are more limited due to the need to mix them in a similar ratio, Agar and Triton-X allowed one to simulate a much broader range of tissue compositions.

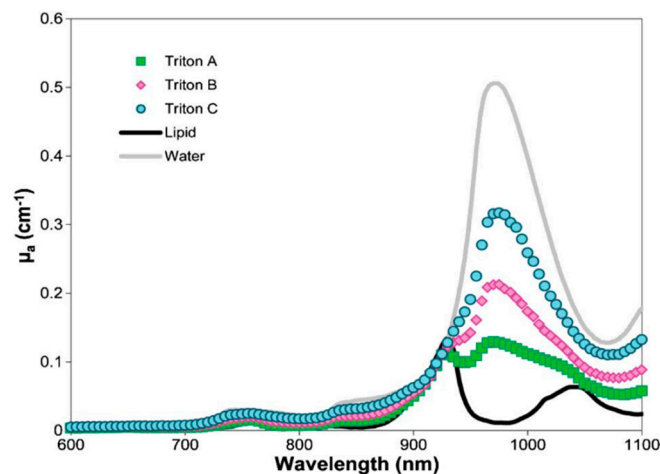


Figure 26. Absorption spectra of different Triton-X-based water/lipid phantoms at different lipid concentrations (A: 70%, B: 50%, C: 30%). For comparison, pure lipid and pure water spectra [186].

In this paper, we have discussed broadband TD-DOS exclusively. An alternative method to measure the same tissue properties is based on frequency domain (FD) recordings of the diffuse light propagating through turbid media such as e.g., human tissue. Frequency domain measurements can be limited to one modulation frequency (as compared to the equivalent of all possible modulation frequencies in TD-DOS), and can thus be conducted with few photons for the same signal-to-noise ratio. This benefit always comes to the expense of less information provided. For some applications, a smaller amount of information might suffice, and then FD measurements may be a good way to go. Frequency domain measurements may be of particular interest if a dynamic event is to be recorded in a homogeneous medium and thus the recording time is limited by the rate of changes in tissue. Another example could be the immediate response of tissue to rapid changes in tissue blood perfusion. However, in most other cases, TD-DOS may be the preferred technique for its much higher informative content. In particular, the depth information is retrieved in a straight forward way by time gating or tagging late photons in time of flight curves. With improving data analysis methods for heterogeneous structures, and with further advances in the development of experimental set-up components, we foresee TD-DOS to address pressing needs like depth sensitivity across various domains of highly scattering media (e.g., optical tomography of deep tissue).

6. Future Outlook

In the last decade, the advancement in source and detector technologies brought in the benefits of considerable cost reduction and miniaturization of broadband time domain instruments as portable devices [41]. Recent studies on small footprint sources and detectors could further promote the miniaturization of TD-DOS towards wearable devices [187,188]. Some initiatives were taken in this direction by EU funded projects. Another key challenge was found in the analysis of heterogeneous media, where recent advances in multi-layer tissue analysis provide hope to further increase the accuracy of analyzed data, thus enabling reliable quantification of tissue constituents in heterogeneous tissue structures [48,152,189]. There is increasing interest in TD-DOS to explore new human tissue types and locations [52,53,190], a further continuation in this direction could add to the exploration and invention of new methodologies to address pressing clinical needs using broadband TD-DOS.

Figure 27 summarizes the current status and future trends in broadband TD-DOS. One trend of growth is foreseen in the extension of broadband TD-DOS to the SWIR region (1000–1900 nm) [121,132]. Though few attempts were made till date, a dedicated approach in this direction would open up many more opportunities as the depth sensitivity could be higher due to relatively low scattering in that wavelength range. The measurement of tissue chromophore performed by broadband TD-DOS could

complement other technologies like an ultrasound for morphological information, elastography to estimate tissue stiffness, diffuse correlation spectroscopy to monitor blood flow. Some exploration is already under progress in this direction [36,187,188,191]. A further push is foreseen in the near future to bring in a multimodal broadband TD-DOS, where the specificity of TD-DOS will be combined with complementary information from other modalities. A preliminary attempt to standardize diffuse optics has been performed in the past [49–51]. Recently, renewed attempts to further strengthen it could bring in the much-needed standards that would harmonize TD-DOS measurements across laboratories [192]. Also, an open data of broadband, well-characterized, stable, reproducibly recipe to make phantom kits, and anatomically correct anthropomorphic tissue phantoms for clinical exploration could further support the cause of standardization [193].

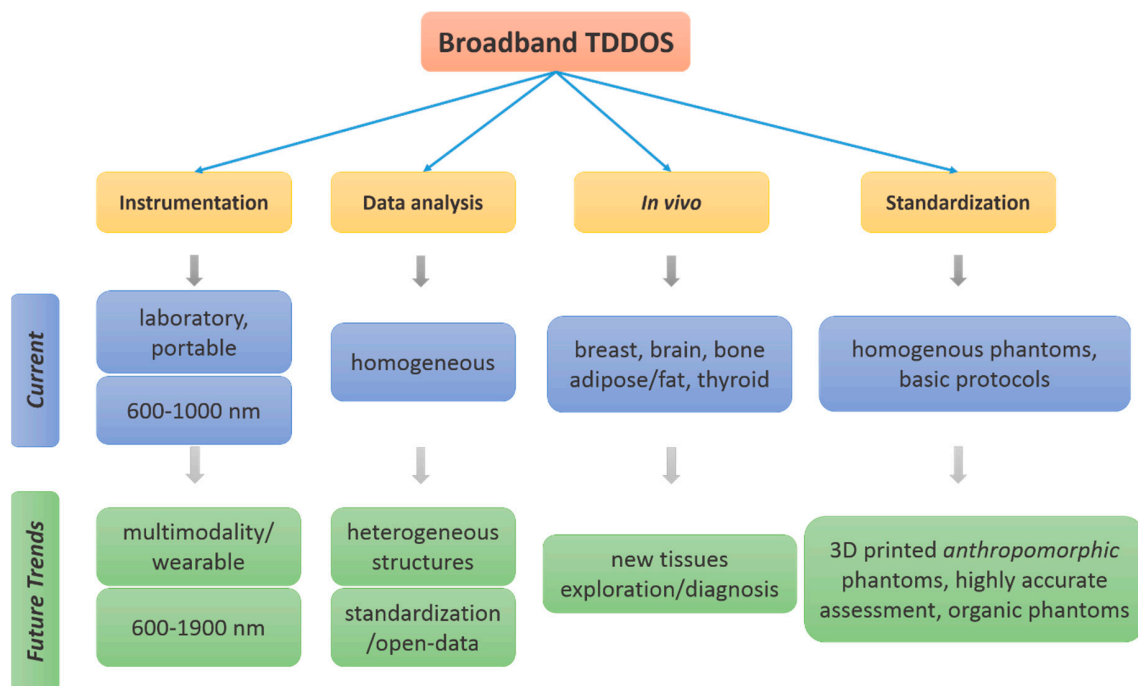


Figure 27. Current explorations and future trends in broadband TD-DOS.

7. Summary and Conclusions

We have presented an up-to-date review in broadband TD-DOS covering various topics of physics, instrumentations, methods of analysis, application to tissue chromophore characterization, in vivo studies, food, wood, pharmaceuticals, and standardization. A renewed focus across the world in biophotonics along with recent advancements in technology could bring further growth in the field. To catalyze this growth, an open data approach and a standardization attempt need to be initiated across laboratories to harvest maximum benefits by harmonizing the measurement protocols. Taking maximum benefits of technological advancements, the vision for the next decade is to push the limits of broadband TD-DOS to bring in small footprint, standardized, multimodal, application-specific TD-DOS devices [41].

Author Contributions: conceptualization, S.K.V.S., A.P. and P.T.; writing—original draft preparation, S.K.V.S., S.A.-E., A.D.M., A.F., P.L., A.P. and P.T.; writing—review and editing, S.K.V.S., S.A.-E., A.D.M., A.F., P.L., A.P. and P.T.

Funding: This review work was funded by Science Foundation Ireland grant no. SFI/15/RP/2828, the European Union’s Horizon 2020 research and innovation programme under grant agreements no. 654148 (Laserlab Europe), No 675332 (BITMAP), No 731877 (SOLUS). BITMAP and SOLUS are an initiative of the Photonics Public-Private Partnership, and Fondazione Cariplo grant no. 2016-1006 (MAYBE).

Acknowledgments: Author thank all the authors of the reprint figures, also the journals for providing permission to reprint the figures in this review.

Conflicts of Interest: The authors declare no conflict of interest.

References

1. Durduran, T.; Choe, R.; Baker, W.B.; Yodh, A.G. Diffuse optics for tissue monitoring and tomography. *Rep. Prog. Phys.* **2010**, *73*, 076701. [[CrossRef](#)] [[PubMed](#)]
2. Nicolai, B.M.; Defraeye, T.; de Ketelaere, B.; Herremans, E.; Hertog, M.L.A.T.M.; Saeys, W.; Torricelli, A.; Vandendriessche, T.; Verboven, P. Nondestructive Measurement of Fruit and Vegetable Quality. *Annu. Rev. Food Sci. Technol.* **2014**, *5*, 285–312. [[CrossRef](#)] [[PubMed](#)]
3. Nicholson, P.H.F.; Lowest, G.; Langton, C.M.; Dequeker, J.; van der Perre, G. A comparison of time-domain and frequency-domain approaches to ultrasonic velocity measurement in trabecular bone. *Phys. Med. Biol.* **1996**, *41*, 2421. [[CrossRef](#)] [[PubMed](#)]
4. Isler, H.; Schenk, D.; Bernhard, J.; Kleiser, S.; Scholkmann, F.; Ostojic, D.; Kalyanov, A.; Ahnen, L.; Wolf, M.; Karen, T. Absorption spectra of early stool from preterm infants need to be considered in abdominal NIRS oximetry. *Biomed. Opt. Express* **2019**, *10*, 2784–2794. [[CrossRef](#)] [[PubMed](#)]
5. Wang, H.; Peng, J.; Xie, C.; Bao, Y.; He, Y. Fruit quality evaluation using spectroscopy technology: A review. *Sensors (Switzerland)* **2015**, *15*, 11889–11927. [[CrossRef](#)] [[PubMed](#)]
6. Dinish, U.S.; Wong, C.L.; Sriram, S.; Ong, W.K.; Balasundaram, G.; Sugii, S.; Olivo, M. Diffuse Optical Spectroscopy and Imaging to Detect and Quantify Adipose Tissue Browning. *Sci. Rep.* **2017**, *7*, 41357. [[CrossRef](#)]
7. Durduran, T.; Yodh, A.G. Diffuse correlation spectroscopy for non-invasive, micro-vascular cerebral blood flow measurement. *Neuroimage* **2014**, *85 Pt 1*, 51–63. [[CrossRef](#)]
8. Gibson, A.P.; Hebden, J.C.; Arridge, S.R. Recent advances in diffuse optical imaging. *Phys. Med. Biol.* **2005**, *50*, R1. [[CrossRef](#)]
9. Deghani, H.; Nivasan, S.S.; Pogue, B.W.; Gibson, A. Numerical modelling and image reconstruction in diffuse optical tomography. *Philos. Trans. R. Soc. A Math. Phys. Eng. Sci.* **2009**, *367*, 3073–3093. [[CrossRef](#)]
10. Zhao, H.; Cooper, R.J. Review of recent progress toward a fiberless, whole-scalp diffuse optical tomography system. *Neurophotonics* **2017**, *5*, 011012. [[CrossRef](#)]
11. Zakharov, P.; Talary, M.S.; Caduff, A. A wearable diffuse reflectance sensor for continuous monitoring of cutaneous blood content. *Phys. Med. Biol.* **2009**, *54*, 5301–5320. [[CrossRef](#)] [[PubMed](#)]
12. Torricelli, A.; Contini, D.; Pifferi, A.; Caffini, M.; Re, R.; Zucchelli, L.; Spinelli, L. Time domain functional NIRS imaging for human brain mapping. *Neuroimage* **2014**, *85 Pt 1*, 28–50. [[CrossRef](#)]
13. Taroni, P.; Paganoni, A.M.; Ieva, F.; Pifferi, A.; Quarto, G.; Abbate, F.; Cassano, E.; Cubeddu, R. Non-invasive optical estimate of tissue composition to differentiate malignant from benign breast lesions: A pilot study. *Sci. Rep.* **2017**, *7*, 40683. [[CrossRef](#)] [[PubMed](#)]
14. Lange, F.; Tachtsidis, I. Clinical brain monitoring with time domain NIRS: A review and future perspectives. *Appl. Sci.* **2019**, *9*, 1612. [[CrossRef](#)]
15. Svensson, T.; Swartling, J.; Taroni, P.; Torricelli, A.; Lindblom, P.; Ingvar, C.; Andersson-Engels, S. Characterization of normal breast tissue heterogeneity using time-resolved near-infrared spectroscopy. *Phys. Med. Biol.* **2005**, *50*, 2559–2571. [[CrossRef](#)]
16. Delpy, D.T.; Cope, M. Quantification in Tissue Near-Infrared Spectroscopy. *Philos. Trans. R. Soc. Lond. Ser. B Biol. Sci.* **1997**, *352*, 649–659. [[CrossRef](#)]
17. Kienle, A.; Forster, F.K.; Hibst, R. Influence of the phase function on determination of the optical properties of biological tissue by spatially resolved reflectance. *Opt. Lett.* **2001**, *26*, 1571–1573. [[CrossRef](#)]
18. Liu, H.; Boas, D.A.; Zhang, Y.; Yodh, A.G.; Chance, B. Determination of optical properties and blood oxygenation in tissue using continuous NIR light. *Phys. Med. Biol.* **1995**, *40*, 1983–1993. [[CrossRef](#)]
19. Scholkmann, F.; Kleiser, S.; Metz, A.J.; Zimmermann, R.; Pavia, J.M.; Wolf, U.; Wolf, M. A review on continuous wave functional near-infrared spectroscopy and imaging instrumentation and methodology. *Neuroimage* **2014**, *85 Pt 1*, 6–27. [[CrossRef](#)]
20. Durduran, T.; Choe, R.; Culver, J.P.; Zubkov, L.; Holboke, M.J.; Giammarco, J.; Chance, B.; Yodh, A.G. Bulk optical properties of healthy female breast tissue. *Phys. Med. Biol.* **2002**, *47*, 2847. [[CrossRef](#)]

21. Pifferi, A.; Farina, A.; Torricelli, A.; Quarto, G.; Cubeddu, R.; Taroni, P. Review: Time-domain broadband near infrared spectroscopy of the female breast: A focused review from basic principles to future perspectives. *J. Near Infrared Spectrosc.* **2012**, *20*, 223–235. [[CrossRef](#)]
22. Pifferi, A.; Torricelli, A.; Taroni, P.; Comelli, D.; Bassi, A.; Cubeddu, R. Fully automated time domain spectrometer for the absorption and scattering characterization of diffusive media. *Rev. Sci. Instrum.* **2007**, *78*, 053103. [[CrossRef](#)] [[PubMed](#)]
23. Konugolu Venkata Sekar, S.; Mora, A.D.; Bargigia, I.; Martinenghi, E.; Lindner, C.; Farzam, P.; Pagliazzi, M.; Durduran, T.; Taroni, P.; Pifferi, A.; et al. Broadband (600–1350 nm) Time-Resolved Diffuse Optical Spectrometer for Clinical Use. *IEEE J. Sel. Top. Quantum Electron.* **2016**, *22*, 7100609. [[CrossRef](#)]
24. Pogue, B.W.; Patterson, M.S. Frequency-domain optical absorption spectroscopy of finite tissue volumes using diffusion theory. *Phys. Med. Biol.* **1994**, *39*, 1157–1180. [[CrossRef](#)]
25. Choe, R.; Putt, M.E.; Carlile, P.M.; Durduran, T.; Giammarco, J.M.; Busch, D.R.; Jung, K.W.; Czerniecki, B.J.; Tchou, J.; Feldman, M.D.; et al. Optically measured microvascular blood flow contrast of malignant breast tumors. *PLoS ONE* **2014**, *9*. [[CrossRef](#)]
26. Pifferi, A.; Torricelli, A.; Taroni, P.; Bassi, A.; Chikoidze, E.; Giambattistelli, E.; Cubeddu, R. Optical biopsy of bone tissue: A step toward the diagnosis of bone pathologies. *J. Biomed. Opt.* **2004**, *9*, 474–481. [[CrossRef](#)]
27. Taroni, P.; Pifferi, A.; Salvagnini, E.; Spinelli, L.; Torricelli, A.; Cubeddu, R. Seven-wavelength time-resolved optical mammography extending beyond 1000 nm for breast collagen quantification. *Opt. Express* **2009**, *17*, 15932–15946. [[CrossRef](#)]
28. Tromberg, B.J.; Pogue, B.W.; Paulsen, K.D.; Yodh, A.G.; Boas, D.A.; Cerussi, A.E. Assessing the future of diffuse optical imaging technologies for breast cancer management. *Med. Phys.* **2008**, *35*, 2443–2451. [[CrossRef](#)]
29. Konugolu Venkata Sekar, S.; Pagliazzi, M.; Negredo, E.; Martelli, F.; Farina, A.; Mora, A.D.; Lindner, C.; Farzam, P.; Pérez-Álvarez, N.; Puig, J.; et al. In Vivo, Non-Invasive Characterization of Human Bone by Hybrid Broadband (600–1200 nm) Diffuse Optical and Correlation Spectroscopies. *PLoS ONE* **2016**, *11*, e0168426. [[CrossRef](#)]
30. Zouaoui, J.; di Sieno, L.; Hervé, L.; Pifferi, A.; Farina, A.; Mora, A.D.; Derouard, J.; Dinten, J.-M. Quantification in time-domain diffuse optical tomography using Mellin-Laplace transforms. *Biomed. Opt. Express* **2016**, *7*, 4346. [[CrossRef](#)]
31. Bale, G.; Mitra, S.; Meek, J.; Robertson, N.; Tachtsidis, I. A new broadband near-infrared spectroscopy system for in-vivo measurements of cerebral cytochrome-c-oxidase changes in neonatal brain injury. *Biomed. Opt. Express* **2014**, *5*, 3450–3466. [[CrossRef](#)] [[PubMed](#)]
32. Pham, T.H.; Coquoz, O.; Fishkin, J.B.; Anderson, E.; Tromberg, B.J. Broad bandwidth frequency domain instrument for quantitative tissue optical spectroscopy. *Rev. Sci. Instrum.* **2000**, *71*, 2500. [[CrossRef](#)]
33. Svensson, T.; Alerstam, E.; Khoptyar, D.; Johansson, J.; Folestad, S.; Andersson-Engels, S. Near-infrared photon time-of-flight spectroscopy of turbid materials up to 1400 nm. *Rev. Sci. Instrum.* **2009**, *80*. [[CrossRef](#)] [[PubMed](#)]
34. Yazdi, H.S.; O'Sullivan, T.D.; Leproux, A.; Hill, B.; Durkin, A.; Telep, S.; Lam, J.; Yazdi, S.S.; Police, A.M.; Carroll, R.M.; et al. Mapping breast cancer blood flow index, composition, and metabolism in a human subject using combined diffuse optical spectroscopic imaging and diffuse correlation spectroscopy. *J. Biomed. Opt.* **2017**, *22*, 045003. [[CrossRef](#)]
35. Kovacsova, Z.; Bale, G.; Veesa, J.D.; Dehghani, H.; Tachtsidis, I. A broadband multi-distance approach to measure tissue oxygen saturation with continuous wave near-infrared spectroscopy. Proceedings of the Diffuse Optical Spectroscopy and Imaging VII, Munich, Germany, 11 July 2019; Volume 11074, p. 110740P.
36. Cortese, L.; Aranda, G.; Buttafava, M.; Contini, D.; Mora, A.D.; de Fraguier, S.; Konugolu Venkata Sekar, S.; Dehghani, H. The LUCA project—Laser and Ultrasound Co-Analyzer for Thyroid Nodules: Overview and Current Status. In *Biophotonics Congress: Biomedical Optics Congress 2018 (Microscopy/Translational/Brain/OTS)*; OSA Technical Digest; Paper OTh4D.5. (n.d.); Optical Society of America: Washington, DC, USA, 2018.
37. Lange, F.; Dunne, L.; Hale, L.; Tachtsidis, I. MAESTROS: A Multiwavelength Time-Domain NIRS System to Monitor Changes in Oxygenation and Oxidation State of Cytochrome-C-Oxidase. *IEEE J. Sel. Top. Quantum Electron.* **2019**, *25*, 7100312. [[CrossRef](#)]
38. Svensson, T.; Alerstam, E.; Einarsdóttir, M.; Svanberg, K.; Andersson-Engels, S. Towards accurate in vivo spectroscopy of the human prostate. *J. Biophotonics* **2008**, *1*, 200–203. [[CrossRef](#)]

39. Svensson, T.; Andersson-Engels, S.; Einarsdóttir, M.; Svanberg, K. In vivo optical characterization of human prostate tissue using near-infrared time-resolved spectroscopy. *J. Biomed. Opt.* **2007**, *12*, 014022. [[CrossRef](#)]
40. Konugolu Venkata Sekar, S. Broadband time-domain diffuse optics for clinical diagnostics, and diffuse Raman spectroscopy. Ph.D. Thesis, Politecnico Milano, Milan, Italy, 2017.
41. Pifferi, A.; Contini, D.; Mora, A.D.; Farina, A.; Spinelli, L.; Torricelli, A. New frontiers in time-domain diffuse optics, a review. *J. Biomed. Opt.* **2016**, *21*, 091310. [[CrossRef](#)]
42. Yamada, Y.; Suzuki, H.; Yamashita, Y. Time-domain near-infrared spectroscopy and imaging: A review. *Appl. Sci.* **2019**, *9*. [[CrossRef](#)]
43. Mora, A.D.; Martinenghi, E.; Contini, D.; Tosi, A.; Boso, G.; Durduran, T.; Arridge, S.; Martelli, F.; Farina, A.; Torricelli, A.; et al. Fast silicon photomultiplier improves signal harvesting and reduces complexity in time-domain diffuse optics. *Opt. Express* **2015**, *23*, 13937–13946. [[CrossRef](#)] [[PubMed](#)]
44. Contini, D.; Mora, A.D.; di Sieno, L.; Cubeddu, R.; Tosi, A.; Boso, G.; Pifferi, A. Memory effect in gated single-photon avalanche diodes: A limiting noise contribution similar to afterpulsing. In *SPIE OPTO*; International Society for Optics and Photonics: Bellingham, WA, USA, 2013; p. 86191L.
45. Zhang, C.; Lindner, S.; Antolovic, I.M.; Wolf, M.; Charbon, E. A CMOS SPAD imager with collision detection and 128 dynamically reallocating TDCs for single-photon counting and 3D time-of-flight imaging. *Sensors (Switzerland)* **2018**, *18*, 4016. [[CrossRef](#)] [[PubMed](#)]
46. Mora, A.D.; Tosi, A.; Contini, D.; di Sieno, L.; Boso, G.; Villa, F.; Pifferi, A. Memory effect in silicon time-gated single-photon avalanche diodes. *J. Appl. Phys.* **2015**, *117*, .
47. Powell, S.; Hochuli, R.; Arridge, S.R. Radiance Monte-Carlo for application of the radiative transport equation in the inverse problem of diffuse optical tomography. In *Optical Tomography and Spectroscopy of Tissue XII*; International Society for Optics and Photonics: Bellingham, WA, USA, 2017; Volume 10059, p. 100590W.
48. Dehghani, H.; Eames, M.E.; Yalavarthy, P.K.; Davis, S.C.; Srinivasan, S.; Carpenter, C.M.; Pogue, B.W.; Paulsen, K.D. Near infrared optical tomography using NIRFAST: Algorithm for numerical model and image reconstruction. *Commun. Numer. Methods Eng.* **2009**, *25*, 711–732. [[CrossRef](#)]
49. Pifferi, A.; Torricelli, A.; Bassi, A.; Taroni, P.; Cubeddu, R.; Wabnitz, H.; Grosenick, D.; Moller, M.; Macdonald, R.; Swartling, J.; et al. Performance assessment of photon migration instruments: The MEDPHOT protocol. *Appl. Opt.* **2005**, *44*, 2104–2114. [[CrossRef](#)]
50. Wabnitz, H.; Jelzow, A.; Mazurenka, M.; Steinkellner, O.; Macdonald, R.; Milej, D.; Zolek, N.; Kacprzak, M.M.; Sawosz, P.; Maniewski, R.; et al. Performance assessment of time-domain optical brain imagers, part 2: nEUROPt protocol. *J. Biomed. Opt.* **2014**, *19*, 86012. [[CrossRef](#)]
51. Wabnitz, H.; Taubert, D.R.; Mazurenka, M.; Steinkellner, O.; Jelzow, A.; Macdonald, R.; Milej, D.; Sawosz, P.; Kacprzak, M.; Liebert, A.; et al. Performance assessment of time-domain optical brain imagers, part 1: Basic instrumental performance protocol. *J. Biomed. Opt.* **2014**, *19*, 86010. [[CrossRef](#)]
52. Konugolu Venkata Sekar, S.; Farina, A.; Martinenghi, E.; Mora, A.D.; Taroni, P.; Pifferi, A.; Negro, E.; Puig, J.; Escrig, R.; Rosales, Q.; et al. Time-resolved diffused optical characterization of key tissue constituents of human bony prominence locations. *Proc. SPIE* **2015**, 9538, 95380X.
53. Konugolu Venkata Sekar, S.; Farina, A.; Mora, A.D.; Taroni, P.; Lindner, C.; Mora, M.; Pagliuzzi, M.; Squarcia, M.; Halperin, I.; Hanzu, F.; et al. Broadband (600–1100 nm) Diffuse Optical Characterization of Thyroid Tissue Constituents and Application to in vivo Thyroid Studies. In *Biophotonics Congress: Biomedical Optics Congress 2018 (Microscopy/Translational/Brain/OTS)*; OSA: Washington, DC, USA, 2018; p. CF2B.3.
54. Sanchez, R.; McCormick, N.J. A Review of Neutron Transport Approximations. *Nucl. Sci. Eng.* **1982**, *80*, 481–535. [[CrossRef](#)]
55. Contini, D.; Martelli, F.; Zaccanti, G. Photon migration through a turbid slab described by a model based on diffusion approximation. I. Theory. *Appl. Opt.* **1997**, *36*, 4587–4599. [[CrossRef](#)]
56. Martelli, F.; Binzoni, T.; Pifferi, A.; Spinelli, L.; Farina, A.; Torricelli, A. There's plenty of light at the bottom: Statistics of photon penetration depth in random media. *Sci. Rep.* **2016**, *6*, 27057. [[CrossRef](#)] [[PubMed](#)]
57. Becker, W. *Advanced Time-Correlated Single Photon Counting Techniques*; Springer Series in Chemical Physics; Springer: New York, NY, USA, 2005.
58. Andersson-Engels, S.; Berg, R.; Persson, A.; Svanberg, S. Multispectral tissue characterization with time-resolved detection of diffusely scattered white light. *Opt. Lett.* **1993**, *18*, 1697. [[CrossRef](#)] [[PubMed](#)]
59. Klinteberg, C.A.; Berg, R.; Lindquist, C.; Andersson-Engels, S.; Svanberg, S. Diffusely scattered femtosecond white-light examination of breast tissue in vitro and in vivo. *Proc. SPIE* **1995**, 2626. [[CrossRef](#)]

60. Abrahamsson, C.; Svensson, T.; Svanberg, S.; Andersson-Engels, S.; Johansson, J.; Folestad, S. Time and wavelength resolved spectroscopy of turbid media using light continuum generated in a crystal fiber. *Opt. Express* **2004**, *12*, 4103–4112. [[CrossRef](#)]
61. Taroni, P.; Pifferi, A.; Torricelli, A.; Comelli, D.; Cubeddu, R. In vivo absorption and scattering spectroscopy of biological tissues. *Photochem. Photobiol. Sci.* **2003**, *2*, 124–129. [[CrossRef](#)]
62. Russell, P. Photonic Crystal Fibers. *Science* **2003**, *299*, 358–362. [[CrossRef](#)]
63. Dudley, J.M.; Taylor, J.R. Ten years of nonlinear optics in photonic crystal fibre. *Nat. Photonics* **2009**, *3*, 85–90. [[CrossRef](#)]
64. Khoptyar, D.; Subash, A.A.; Johansson, S.; Saleem, M.; Sparén, A.; Johansson, J.; Andersson-Engels, S. Broadband photon time-of-flight spectroscopy of pharmaceuticals and highly scattering plastics in the VIS and close NIR spectral ranges. *Opt. Express* **2013**, *21*, 20941–20953. [[CrossRef](#)]
65. Grigoriev, E.; Akindinov, A.; Breitenmoser, M.; Buono, S.; Charbon, E.; Niclass, C.; Desforges, I.; Rocca, R. Silicon photomultipliers and their bio-medical applications. *Nucl. Instrum. Methods Phys. Res. Sect. A Accel. Spectrometers Detect. Assoc. Equip.* **2007**, *571*, 130–133. [[CrossRef](#)]
66. Farina, A.; Tagliabue, S.; di Sieno, L.; Martinenghi, E.; Durduran, T.; Arridge, S.; Martelli, F.; Torricelli, A.; Pifferi, A.; Mora, A.D. Time-domain functional diffuse optical tomography system based on fiber-free silicon photomultipliers. *Appl. Sci.* **2017**, *7*, 1235.
67. Konugolu Venkata Sekar, S.; Farina, A.; Martinenghi, E.; Mora, A.D.; Taroni, P.; Pifferi, A.; Durduran, T.; Pagliuzzi, M.; Lindner, C.; Farzam, P.; et al. Broadband time-resolved diffuse optical spectrometer for clinical diagnostics: Characterization and in-vivo measurements in the 600–1350 nm spectral range. In *European Conference on Biomedical Optics*; Optical Society of America: Washington, DC, USA, 2015; p. 95380R.
68. Konugolu Venkata Sekar, S.; Farina, A.; Mora, A.D.; Taroni, P.; Lindner, C.; Mora, M.; Farzam, P.; Pagliuzzi, M.; Squarcia, M.; Halperin, I.; et al. Thyroid tissue constituents characterization and application to in vivo studies by broadband (600–1200 nm) diffuse optical spectroscopy. In *European Conference on Biomedical Optics*; Optical Society of America: Washington, DC, USA, 2017; p. 1041107.
69. Bassi, A.; Swartling, J.; D'Andrea, C.; Pifferi, A.; Torricelli, A.; Cubeddu, R. Time-resolved spectrophotometer for turbid media based on supercontinuum generation in a photonic crystal fiber. *Opt. Lett.* **2004**, *29*, 2405–2407. [[CrossRef](#)] [[PubMed](#)]
70. Gerega, A.; Milej, D.; Weigl, W.; Kacprzak, M.; Liebert, A. Multiwavelength time-resolved near-infrared spectroscopy of the adult head: Assessment of intracerebral and extracerebral absorption changes. *Biomed. Opt. Express* **2018**, *9*, 2974. [[CrossRef](#)] [[PubMed](#)]
71. Terborg, C.; Bramer, S.; Harscher, S.; Simon, M.; Witte, O.W. Bedside assessment of cerebral perfusion reductions in patients with acute ischaemic stroke by near-infrared spectroscopy and indocyanine green. *J. Neurol. Neurosurg. Psychiatry* **2004**, *75*, 38–42. [[PubMed](#)]
72. Milej, D.; Abdalmalak, A.; Desjardins, L.; Ahmed, H.; Lee, T.Y.; Diop, M.; Lawrence, K.S. Quantification of blood-brain barrier permeability by dynamic contrast-enhanced NIRS. *Sci. Rep.* **2017**, *7*, 1702. [[CrossRef](#)] [[PubMed](#)]
73. Liebert, A.; Wabnitz, H.; Steinbrink, J.; Möller, M.; Macdonald, R.; Rinneberg, H.; Villringer, A.; Obrig, H. Bed-side assessment of cerebral perfusion in stroke patients based on optical monitoring of a dye bolus by time-resolved diffuse reflectance. *Neuroimage* **2005**, *24*, 426–435. [[CrossRef](#)] [[PubMed](#)]
74. Weigl, W.; Milej, D.; Gerega, A.; Toczyłowska, B.; Kacprzak, M.; Sawosz, P.; Botwicz, M.; Maniewski, R.; Mayzner-Zawadzka, E.; Liebert, A. Assessment of cerebral perfusion in post-traumatic brain injury patients with the use of ICG-bolus tracking method. *Neuroimage* **2014**, *85*, 555–565. [[CrossRef](#)] [[PubMed](#)]
75. Weigl, W.; Milej, D.; Gerega, A.; Toczyłowska, B.; Sawosz, P.; Kacprzak, M.; Janusek, D.; Wojtkiewicz, S.; Maniewski, R.; Liebert, A. Confirmation of brain death using optical methods based on tracking of an optical contrast agent: Assessment of diagnostic feasibility. *Sci. Rep.* **2018**, *8*, 7332. [[CrossRef](#)]
76. Hawrysz, D.J.; Sevic-Muraca, E.M. Developments toward diagnostic breast cancer imaging using near-infrared optical measurements and fluorescent contrast agents. *Neoplasia* **2000**, *2*, 388–417. [[CrossRef](#)]
77. Ishizawa, T.; Fukushima, N.; Shibahara, J.; Masuda, K.; Tamura, S.; Aoki, T.; Hasegawa, K.; Beck, Y.; Fukayama, M.; Kokudo, N. Real-time identification of liver cancers by using indocyanine green fluorescent imaging. *Cancer* **2009**, *115*, 2491–2504.

78. Contini, D.; Martelli, F.; Zaccanti, G. Photon migration through a turbid slab described by a model based on diffusion approximation. I. Comparison with Monte Carlo Results. *Appl. Opt.* **1997**, *36*, 4600–4612. [[CrossRef](#)] [[PubMed](#)]
79. Liemert, A.; Martelli, F.; Binzoni, T.; Kienle, A. P₃ solution for the total steady-state and time-resolved reflectance and transmittance from a turbid slab. *Appl. Opt.* **2019**, *58*, 4143. [[CrossRef](#)] [[PubMed](#)]
80. Liemert, A.; Reitzle, D.; Kienle, A. Analytical solutions of the radiative transport equation for turbid and fluorescent layered media. *Sci. Rep.* **2017**, *7*, 3819. [[CrossRef](#)] [[PubMed](#)]
81. Liemert, A.; Kienle, A. Light diffusion in a turbid cylinder. II. Layered case. *Opt. Express* **2010**, *18*, 9266–9279. [[CrossRef](#)] [[PubMed](#)]
82. Kienle, A. Light diffusion through a turbid parallelepiped. *J. Opt. Soc. Am. A* **2005**, *22*, 1883–1888. [[CrossRef](#)]
83. Simpson, C.R.; Kohl, M.; Essenpreis, M.; Cope, M. Near-infrared optical properties of ex vivo human skin and subcutaneous tissues measured using the Monte Carlo inversion technique. *Phys. Med. Biol.* **1998**, *43*, 2465–2478. [[CrossRef](#)]
84. Sassaroli, A.; Martelli, F.; Zaccanti, G.; Yamada, Y. Performance of Fitting Procedures in Curved Geometry for Retrieval of the Optical Properties of Tissue from Time-Resolved Measurements. *Appl. Opt.* **2001**, *40*, 185–197. [[CrossRef](#)]
85. Kamran, F.; Abildgaard, O.H.A.; Subash, A.A.; Andersen, P.E.; Andersson-Engels, S.; Khoptyar, D. Computationally effective solution of the inverse problem in time-of-flight spectroscopy. *Opt. Express* **2015**, *23*, 6937–6945. [[CrossRef](#)]
86. Martelli, F.; Bassani, M.; Alianelli, L.; Zangheri, L.; Zaccanti, G. Accuracy of the diffusion equation to describe photon migration through an infinite medium: Numerical and experimental investigation. *Phys. Med. Biol.* **2000**, *45*, 1359–1373. [[CrossRef](#)]
87. Schweiger, M.; Arridge, S.R. The finite-element method for the propagation of light in scattering media: Frequency domain case. *Med. Phys.* **1997**, *24*, 895–902. [[CrossRef](#)]
88. Schweiger, M.; Arridge, S. The Toast ++ software suite for forward and inverse modeling in optical tomography. *J. Biomed. Opt.* **2014**, *19*, 040801. [[CrossRef](#)] [[PubMed](#)]
89. Wojtkiewicz, S.; Durduran, T.; Dehghani, H. Time-resolved near infrared light propagation using frequency domain superposition. *Biomed. Opt. Express* **2018**, *9*, 41–54. [[CrossRef](#)] [[PubMed](#)]
90. Wang, L.; Jacques, S.L.; Zheng, L. MCML—Monte Carlo modeling of light transport in multi-layered tissues. *Comput. Methods Programs Biomed.* **1995**, *47*, 131–146.
91. Sassaroli, A.; Martelli, F. Equivalence of four Monte Carlo methods for photon migration in turbid media. *J. Opt. Soc. Am. A. Opt. Image Sci. Vis.* **2012**, *29*, 2110–2117. [[CrossRef](#)] [[PubMed](#)]
92. Alerstam, E.; Svensson, T.; Andersson-Engels, S. Parallel computing with graphics processing units for high-speed Monte Carlo simulation of photon migration. *J. Biomed. Opt.* **2008**, *13*, 060504. [[PubMed](#)]
93. Fang, Q.; Kaeli, D.R. Accelerating mesh-based Monte Carlo method on modern CPU architectures. *Biomed. Opt. Express* **2012**, *3*, 3223–3230. [[CrossRef](#)]
94. Yao, R.; Intes, X.; Fang, Q. Generalized mesh-based Monte Carlo for wide-field illumination and detection via mesh retessellation. *Biomed. Opt. Express* **2015**, *7*, 171. [[CrossRef](#)]
95. Fang, Q. Mesh-based Monte Carlo method using fast ray-tracing in Plücker coordinates. *Biomed. Opt. Express* **2010**, *1*, 165–175.
96. Alerstam, E.; Andersson-Engels, S.; Svensson, T. White Monte Carlo for time-resolved photon migration. *J. Biomed. Opt.* **2008**, *13*, 041304.
97. Alerstam, E.; Andersson-Engels, S.; Svensson, T. Improved accuracy in time-resolved diffuse reflectance spectroscopy. *Opt. Express* **2008**, *16*, 10434–10448. [[CrossRef](#)]
98. Selb, J.; Ogden, T.M.; Dubb, J.; Fang, Q.; Boas, D.A. Systematic evaluation of a time-domain Monte Carlo fitting routine to estimate the adult brain optical properties. In *Optical Tomography and Spectroscopy of Tissue X*; International Society for Optics and Photonics: Bellingham, WA, USA, 2013; Volume 8578, p. 857817.
99. Arridge, S.R. Photon-measurement density functions. Part I: Analytical forms. *Appl. Opt.* **1995**, *34*, 7395–7409. [[CrossRef](#)] [[PubMed](#)]
100. Arridge, S.R.; Schweiger, M. Photon-measurement density functions. Part 2: Finite-element-method calculations. *Appl. Opt.* **1995**, *34*, 8026–8037. [[CrossRef](#)] [[PubMed](#)]
101. Martelli, F.; del Bianco, S.; Ismaelli, A.; Zaccanti, G. *Light Propagation through Biological Tissue and Other Diffusive Media*; SPIE Press: Bellingham, WA, USA, 2010.

102. Martelli, F.; del Bianco, S.; di Ninni, P. Perturbative forward solver software for small localized fluorophores in tissue. *Biomed. Opt. Express* **2012**, *3*, 26. [[CrossRef](#)] [[PubMed](#)]
103. Torricelli, A.; Spinelli, L.; Pifferi, A.; Taroni, P.; Cubeddu, R.; Danesini, G. Use of a nonlinear perturbation approach for in vivo breast lesion characterization by multiwavelength time-resolved optical mammography. *Opt. Express* **2003**, *11*, 853–867. [[CrossRef](#)] [[PubMed](#)]
104. Martelli, F.; Pifferi, A.; Contini, D.; Spinelli, L.; Torricelli, A.; Wabnitz, H.; Macdonald, R.; Sassaroli, A.; Zaccanti, G. Phantoms for diffuse optical imaging based on totally absorbing objects, part 1: Basic concepts. *J. Biomed. Opt.* **2013**, *18*, 66014. [[CrossRef](#)] [[PubMed](#)]
105. Sassaroli, A.; Pifferi, A.; Contini, D.; Torricelli, A.; Spinelli, L.; Wabnitz, H.; di Ninni, P.; Zaccanti, G.; Martelli, F. Forward solvers for photon migration in the presence of highly and totally absorbing objects embedded inside diffusive media. *J. Opt. Soc. Am. A* **2014**, *31*, 460. [[CrossRef](#)]
106. Sassaroli, A.; Blumetti, C.; Martelli, F.; Alianelli, L.; Contini, D.; Ismaelli, A.; Zaccanti, G. Monte carlo procedure for investigating light propagation and imaging of highly scattering media. *Appl. Opt.* **1998**, *37*, 7392–7400. [[CrossRef](#)]
107. Sassaroli, A. Fast perturbation Monte Carlo method for photon migration in heterogeneous turbid media. *Opt. Lett.* **2011**, *36*, 2095–2097. [[CrossRef](#)]
108. Nguyen, J.; Hayakawa, C.K.; Mourant, J.R.; Spanier, J. Perturbation Monte Carlo methods for tissue structure alterations. *Biomed. Opt. Express* **2013**, *4*, 1946–1963. [[CrossRef](#)]
109. Chauchard, F.; Roger, J.M.; Bellon-Maurel, V.; Abrahamsson, C.; Andersson-Engels, S.; Svanberg, S. MADSTRESS: A linear approach for evaluating scattering and absorption coefficients of samples measured using time-resolved spectroscopy in reflection. *Appl. Spectrosc.* **2005**, *59*, 1229–1235. [[CrossRef](#)]
110. Chauchard, F.; Roussel, S.; Roger, J.M.; Bellon-Maurel, V.; Abrahamsson, C.; Svensson, T.; Andersson-Engels, S.; Svanberg, S. Least-squares support vector machines modelization for time-resolved spectroscopy. *Appl. Opt.* **2005**, *44*, 7091–7097. [[CrossRef](#)] [[PubMed](#)]
111. Mourant, J.R.; Fuselier, T.; Boyer, J.; Johnson, T.M.T.M.; Bigio, I.J.I.J. Predictions and measurements of scattering and absorption over broad wavelength ranges in tissue phantoms. *Appl. Opt.* **1997**, *36*, 949. [[CrossRef](#)] [[PubMed](#)]
112. Nilsson, A.M.; Stureson, C.; Liu, D.L.; Andersson-Engels, S. Changes in spectral shape of tissue optical properties in conjunction with laser-induced thermotherapy. *Appl. Opt.* **1998**, *37*, 1256–1267. [[CrossRef](#)] [[PubMed](#)]
113. D'Andrea, C.; Spinelli, L.; Bassi, A.; Giusto, A.; Contini, D.; Swartling, J.; Torricelli, A.; Cubeddu, R. Time-resolved spectrally constrained method for the quantification of chromophore concentrations and scattering parameters in diffusing media. *Opt. Express* **2006**, *14*, 1888–1898. [[CrossRef](#)]
114. Farina, A.; Bassi, A.; Pifferi, A.; Taroni, P.; Comelli, D.; Spinelli, L.; Cubeddu, R. Bandpass effects in time-resolved diffuse spectroscopy. *Appl. Spectrosc.* **2009**, *63*, 48–56. [[CrossRef](#)]
115. Guggenheim, J.A.; Bargigia, I.; Farina, A.; Pifferi, A.; Dehghani, H. Time resolved diffuse optical spectroscopy with geometrically accurate models for bulk parameter recovery. *Biomed. Opt. Express* **2016**, *7*, 3784. [[CrossRef](#)]
116. Bouchard, J.; Veilleux, I.; Jedidi, R.; Noiseux, I.; Fortin, M.; Mermut, O. Reference optical phantoms for diffuse optical spectroscopy. Part 1—Error analysis of a time resolved transmittance characterization method. *Opt. Express* **2010**, *18*, 1143–1155. [[CrossRef](#)]
117. Martelli, F.; del Bianco, S.; Zaccanti, G. Retrieval procedure for time-resolved near-infrared tissue spectroscopy based on the optimal estimation method. *Phys. Med. Biol.* **2012**, *57*, 2915–2929. [[CrossRef](#)]
118. Martelli, F.; del Bianco, S.; Spinelli, L.; Cavalieri, S.; di Ninni, P.; Binzoni, T.; Jelzow, A.; Macdonald, R.; Wabnitz, H. Optimal estimation reconstruction of the optical properties of a two-layered tissue phantom from time-resolved single-distance measurements. *J. Biomed. Opt.* **2015**, *20*, 115001. [[CrossRef](#)]
119. Konugolu Venkata Sekar, S.; Farina, A.; Mora, A.D.; Lindner, C.; Pagliuzzi, M.; Mora, M.; Aranda, G.; Dehghani, H.; Durduran, T.; Taroni, P.; et al. Broadband (550–1350 nm) diffuse optical characterization of thyroid chromophores. *Sci. Rep.* **2018**, *8*, 10015. [[CrossRef](#)] [[PubMed](#)]
120. Nachabé, R.; Evers, D.J.; Hendriks, B.H.W.; Lucassen, G.W.; van der Voort, M.; Rutgers, E.J.; Peeters, M.-J.V.; van der Hage, J.a.; Oldenburg, H.S.; Wesseling, J.; et al. Diagnosis of breast cancer using diffuse optical spectroscopy from 500 to 1600 nm: Comparison of classification methods. *J. Biomed. Opt.* **2011**, *16*, 087010. [[CrossRef](#)] [[PubMed](#)]

121. Konugolu Venkata Sekar, S.; Bargigia, I.; Mora, A.D.; Taroni, P.; Ruggeri, A.; Tosi, A.; Pifferi, A.; Farina, A. Diffuse optical characterization of collagen absorption from 500 to 1700 nm. *J. Biomed. Opt.* **2017**, *22*, 15006. [[CrossRef](#)] [[PubMed](#)]
122. Provenzano, P.P.; Inman, D.R.; Eliceiri, K.W.; Knittel, J.G.; Yan, L.; Rueden, C.T.; White, J.G.; Keely, P.J. Collagen density promotes mammary tumor initiation and progression. *BMC Med.* **2008**, *6*, 11. [[CrossRef](#)] [[PubMed](#)]
123. Taroni, P.; Quarto, G.; Pifferi, A.; Ieva, F.; Paganoni, A.M.; Abbate, F.; Balestreri, N.; Menna, S.; Cassano, E.; Cubeddu, R. Optical identification of subjects at high risk for developing breast cancer. *J. Biomed. Opt.* **2013**, *18*, 060507. [[CrossRef](#)]
124. Taroni, P.; Comelli, D.; Pifferi, A.; Torricelli, A.; Cubeddu, R. Absorption of collagen: Effects on the estimate of breast composition and related diagnostic implications. *J. Biomed. Opt.* **2007**, *12*, 014021. [[CrossRef](#)]
125. Taroni, P.; Bassi, A.; Comelli, D.; Farina, A.; Cubeddu, R.; Pifferi, A. Diffuse optical spectroscopy of breast tissue extended to 1100 nm. *J. Biomed. Opt.* **2009**, *14*, 054030. [[CrossRef](#)]
126. Puschmann, S.; Rahn, C.-D.; Wenck, H.; Gallinat, S.; Fischer, F. Approach to quantify human dermal skin aging using multiphoton laser scanning microscopy. *J. Biomed. Opt.* **2012**, *17*, 036005. [[CrossRef](#)]
127. Sinkus, R.; Lorenzen, J.; Schrader, D.; Lorenzen, M.; Dargatz, M.; Holz, D. High-resolution tensor MR elastography for breast tumour detection. *Phys. Med. Biol.* **2000**, *45*, 1649–1664. [[CrossRef](#)]
128. Plewes, D.B.; Bishop, J.; Samani, A.; Sciarretta, J. Visualization and quantification of breast cancer biomechanical properties with magnetic resonance elastography. *Phys. Med. Biol.* **2000**, *45*, 1591–1610. [[CrossRef](#)]
129. Konugolu Venkata Sekar, S.; Beh, J.S.; Farina, A.; Mora, A.D.; Pifferi, A.; Taroni, P. Broadband diffuse optical characterization of elastin for biomedical applications. *Biophys. Chem.* **2017**, *229*, 130–134. [[CrossRef](#)]
130. Bremer, A.A.; Jialal, I. Adipose tissue dysfunction in nascent metabolic syndrome. *J. Obes.* **2013**, *2013*. [[CrossRef](#)] [[PubMed](#)]
131. Bremer, A.A.; Devaraj, S.; Afify, A.; Jialal, I. Adipose Tissue Dysregulation in Patients with Metabolic Syndrome. *J. Clin. Endocrinol. Metab.* **2011**, *96*, E1782–E1788. [[CrossRef](#)] [[PubMed](#)]
132. Bargigia, I.; Tosi, A.; Shehata, A.B.; della Frera, A.; Farina, A.; Bassi, A.; Taroni, P.; Mora, A.D.; Zappa, F.; Cubeddu, R.; et al. Time-resolved diffuse optical spectroscopy up to 1700 nm by means of a time-gated InGaAs/InP single-photon avalanche diode. *Appl. Spectrosc.* **2012**, *66*, 944–950. [[CrossRef](#)] [[PubMed](#)]
133. Lindner, C.; Mora, M.; Farzam, P.; Squarcia, M.; Johansson, J.; Weigel, U.M.; Halperin, I.; Hanzu, F.A.; Durduran, T. Diffuse optical characterization of the healthy human thyroid tissue and two pathological case studies. *PLoS ONE* **2016**, *11*, e0147851. [[CrossRef](#)] [[PubMed](#)]
134. Taroni, P.; Pifferi, A.; Quarto, G.; Spinelli, L.; Torricelli, A.; Abbate, F.; Villa, A.; Balestreri, N.; Menna, S.; Cassano, E.; et al. Noninvasive assessment of breast cancer risk using time-resolved diffuse optical spectroscopy. *J. Biomed. Opt.* **2010**, *15*, 060501. [[CrossRef](#)] [[PubMed](#)]
135. Farina, A.; Torricelli, A.; Bargigia, I.; Spinelli, L.; Cubeddu, R.; Foschum, F.; Jäger, M.; Simon, E.; Fugger, O.; Kienle, A.; et al. In-vivo multilaboratory investigation of the optical properties of the human head. *Biomed. Opt.* **2014**, *6*, 2609–2623.
136. Liemert, A.; Kienle, A. Exact and efficient solution of the radiative transport equation for the semi-infinite medium. *Sci. Rep.* **2013**, *3*, 2018. [[CrossRef](#)]
137. Geiger, S.; Reitzle, D.; Liemert, A.; Kienle, A. Determination of the optical properties of three-layered turbid media in the time domain using the P_3 approximation. *OSA Contin.* **2019**, *2*, 1889. [[CrossRef](#)]
138. Konugolu Venkata Sekar, S.; Mora, A.D.; Martinenghi, E.; Taroni, P.; Farina, A.; Puig, J.; Negro, E.; Lindner, C.; Pagliuzzi, M. In vivo Time domain Broadband (600–1200 nm) Diffuse Optical Characterization of Human Bone. In *Optical Tomography and Spectroscopy*; Optical Society of America: Washington, DC, USA, 2016; p. JTU3A.32.
139. Tee, Y.Y.; Lowe, A.J.; Brand, C.A.; Judson, R.T. Fine-Needle Aspiration May Miss a Third of All Malignancy in Palpable Thyroid Nodules. *Ann. Surg.* **2007**, *246*, 714–720. [[CrossRef](#)]
140. Giordano, A.; Frontini, A.; Cinti, S. Convertible visceral fat as a therapeutic target to curb obesity. *Nat. Rev. Drug Discov.* **2016**, *15*, 405–424. [[CrossRef](#)]
141. Ganesan, G.; Warren, R.V.; Leproux, A.; Compton, M.; Cutler, K.; Wittkopp, S.; Tran, G.; O'Sullivan, T.; Malik, S.; Galassetti, P.R.; et al. Diffuse optical spectroscopic imaging of subcutaneous adipose tissue metabolic changes during weight loss. *Int. J. Obes.* **2016**, *40*, 1292–1300. [[CrossRef](#)] [[PubMed](#)]

142. Torricelli, A.; Pifferi, A.; Taroni, P.; Giambattistelli, E.; Cubeddu, R. In vivo optical characterization of human tissues from 610 to 1010 nm by time-resolved reflectance spectroscopy. *Phys. Med. Biol.* **2001**, *46*, 2227–2237. [[CrossRef](#)] [[PubMed](#)]
143. Pifferi, A.; Konugolu Venkata Sekar, S.; Farina, A.; Guadagno, C.; Spinelli, L.; Lanka, P.; Cubeddu, R.; Nisoli, E.; Taroni, P. In vivo Study of the Layered Structure on the Abdomen by Broadband Time-Domain Diffuse Optical Spectroscopy. In *Optical Tomography and Spectroscopy*; Optical Society of America: Washington, DC, USA, 2018.
144. Kelley, S.S.; Rials, T.G.; Snell, R.; Groom, L.H.; Sluiter, A. Use of near infrared spectroscopy to measure the chemical and mechanical properties of solid wood. *Wood Sci. Technol.* **2004**, *38*, 257–276. [[CrossRef](#)]
145. Tsuchikawa, S. A review of recent near infrared research for wood and paper. *Appl. Spectrosc. Rev.* **2007**. [[CrossRef](#)]
146. Hodge, G.R.; Woodbridge, W.C. Global near infrared models to predict lignin and cellulose content of pine wood. *J. Near Infrared Spectrosc.* **2010**, *18*, 367–380. [[CrossRef](#)]
147. Tsuchikawa, S.; Schwanninger, M. A review of recent near-infrared research for wood and paper (Part 2). *Appl. Spectrosc. Rev.* **2013**, *48*, 560–587. [[CrossRef](#)]
148. Sandak, A.; Sandak, J.; Zborowska, M.; Pradzyński, W. Near infrared spectroscopy as a tool for archaeological wood characterization. *J. Archaeol. Sci.* **2010**, *37*, 2093–2101. [[CrossRef](#)]
149. D'Andrea, C.; Farina, A.; Comelli, D.; Pifferi, A.; Taroni, P.; Valentini, G.; Cubeddu, R.; Zoia, L.; Orlandi, M.; Kienle, A. Time-resolved optical spectroscopy of wood. *Appl. Spectrosc.* **2008**, *62*, 569–574. [[CrossRef](#)]
150. D'Andrea, C.; Nevin, A.; Farina, A.; Bassi, A.; Cubeddu, R. Assessment of variations in moisture content of wood using time-resolved diffuse optical spectroscopy. *Appl. Opt.* **2009**, *48*, B87–B93. [[CrossRef](#)]
151. Farina, A.; Bargigia, I.; Janeček, E.-R.; Walsh, Z.; D'Andrea, C.; Nevin, A.; Ramage, M.; Scherman, O.A.; Pifferi, A. Nondestructive optical detection of monomer uptake in wood polymer composites. *Opt. Lett.* **2014**, *39*, 228–231. [[CrossRef](#)]
152. Janeček, E.R.; Walsh-Korb, Z.; Bargigia, I.; Farina, A.; Ramage, M.H.; D'Andrea, C.; Nevin, A.; Pifferi, A.; Scherman, O.A. Time-resolved laser spectroscopy for the in situ characterization of methacrylate monomer flow within spruce. *Wood Sci. Technol.* **2017**, *51*, 227–242. [[CrossRef](#)]
153. Zude, M.; Herold, B.; Roger, J.M.; Bellon-Maurel, V.; Landahl, S. Non-destructive tests on the prediction of apple fruit flesh firmness and soluble solids content on tree and in shelf life. *J. Food Eng.* **2006**, *77*, 254–260. [[CrossRef](#)]
154. Qing, Z.; Ji, B.; Zude, M. Predicting soluble solid content and firmness in apple fruit by means of laser light backscattering image analysis. *J. Food Eng.* **2007**, *82*, 58–67. [[CrossRef](#)]
155. Cubeddu, R.; D'Andrea, C.; Pifferi, A.; Taroni, P.; Torricelli, A.; Valentini, G.; Dover, C.; Johnson, D.; Ruiz-Altisent, M.; Valero, C. Nondestructive quantification of chemical and physical properties of fruits by time-resolved reflectance spectroscopy in the wavelength range 650–1000 nm. *Appl. Opt.* **2001**, *40*, 538–543. [[CrossRef](#)] [[PubMed](#)]
156. Nicolaï, B.M.; Verlinden, B.E.; Desmet, M.; Saevels, S.; Saeys, W.; Theron, K.; Cubeddu, R.; Pifferi, A.; Torricelli, A. Time-resolved and continuous wave NIR reflectance spectroscopy to predict soluble solids content and firmness of pear. *Postharvest Biol. Technol.* **2008**, *47*, 68–74. [[CrossRef](#)]
157. Cubeddu, R.; D'Andrea, C.; Pifferi, A.; Taroni, P.; Torricelli, A.; Valentini, G.; Ruiz-Altisent, M.; Valero, C.; Ortiz, C.; Dover, C.; et al. Time-resolved reflectance spectroscopy applied to the nondestructive monitoring of the internal optical properties in apples. *Appl. Spectrosc.* **2001**, *55*, 1368–1374. [[CrossRef](#)]
158. Nielsen, O.H.A.; Subash, A.A.; Nielsen, F.D.; Dahl, A.B.; Skytte, J.L.; Andersson-Engels, S.; Khoptyar, D. Spectral characterisation of dairy products using photon time-of-flight spectroscopy. *J. Near Infrared Spectrosc.* **2013**, *21*, 375–383. [[CrossRef](#)]
159. Khoptyar, D.; Kamran, F.; Nielsen, O.H.; Sparén, A.; Johansson, J.; Svensson, O.; Andersson-Engels, S. Broadband photon time of flight spectroscopy: Advanced spectroscopic tool for PAT in pharmaceutical and dairy industries. In *Asia Communications and Photonics Conference*; Optical Society of America: Washington, DC, USA, 2014.
160. Kamran, F. Quality Assessment of Turbid Media: Milk and Pharmaceuticals. Ph.D. Thesis, Technical University of Denmark (DTU), København, Denmark, 2014.
161. Johansson, S. Broadband Photon Time-of-Flight Spectroscopy on Pharmaceutical Tablets and Dairy Products. In *Lund Reports on Atomic Physics*; Lund University: Lund, Sweden, 2014.

162. Svensson, T.; Andersson, M.; Rippe, L.; Svanberg, S.; Andersson-Engels, S.; Johansson, J.; Folestad, S. VCSEL-based oxygen spectroscopy for structural analysis of pharmaceutical solids. *Appl. Phys. B Lasers Opt.* **2008**, *90*, 345–354. [[CrossRef](#)]
163. Johansson, J.; Folestad, S.; Josefson, M.; Sparen, A.; Abrahamsson, C.; Andersson-Engels, S.; Svanberg, S. Time-resolved NIR/vis spectroscopy for analysis of solids: Pharmaceutical tablets. *Appl. Spectrosc.* **2002**, *56*, 725–731. [[CrossRef](#)]
164. Abrahamsson, C.; Johansson, J.; Andersson-Engels, S.; Svanberg, S.; Folestad, S. Time-resolved NIR spectroscopy for quantitative analysis of intact pharmaceutical tablets. *Anal. Chem.* **2005**, *77*, 1055–1059. [[CrossRef](#)] [[PubMed](#)]
165. Abrahamsson, C.; Löwgren, A.; Strömdahl, B.; Svensson, T.; Andersson-Engels, S.; Johansson, J.; Folestad, S. Scatter correction of transmission near-infrared spectra by photon migration data: Quantitative analysis of solids. *Appl. Spectrosc.* **2005**, *59*, 1381–1387. [[CrossRef](#)] [[PubMed](#)]
166. Svensson, T.; Persson, L.; Andersson, M.; Svanberg, S.; Andersson-Engels, S.; Johansson, J.; Folestad, S. Noninvasive characterization of pharmaceutical solids by diode laser oxygen spectroscopy. *Appl. Spectrosc.* **2007**. [[CrossRef](#)] [[PubMed](#)]
167. Subash, A.A. Wide-Bandwidth Time of Flight Spectroscopy of Turbid Media. sweden. *Lund Rep. At. Phys.* **2011**, *61*, 784–786.
168. Abrahamsson, C. *Time-Resolved Spectroscopy for Pharmaceutical Applications*; Lund Institute of Technology, Lund University: Lund, Sweden, 2005.
169. Kamran, F.; Abildgaard, O.H.A.; Sparén, A.; Svensson, O.; Johansson, J.; Andersson-Engels, S.; Andersen, P.E.; Khoptyar, D. Transmission near-infrared (NIR) and photon time-of-flight (PTOF) spectroscopy in a comparative analysis of pharmaceuticals. *Appl. Spectrosc.* **2015**, *69*, 389–397. [[CrossRef](#)]
170. Editorial, Keeping up standards. *Nat. Photonics* **2018**, *12*, 117. [[CrossRef](#)]
171. Di Sieno, L.; Nissinen, J.; Hallman, L.; Martinenghi, E.; Contini, D.; Pifferi, A.; Kostamovaara, J.; Mora, A.D. Miniaturized pulsed laser source for time-domain diffuse optics routes to wearable devices. *J. Biomed. Opt.* **2017**, *22*, 1–9. [[CrossRef](#)]
172. Martinenghi, E.; Mora, A.D.; Contini, D.; Farina, A.; Villa, F.; Torricelli, A.; Pifferi, A. Spectrally Resolved Single-Photon Timing of Silicon Photomultipliers for Time-Domain Diffuse Spectroscopy. *IEEE Photonics J.* **2015**, *7*, 1–12. [[CrossRef](#)]
173. Tyndall, D.; Rae, B.; Li, D.; Richardson, J.; Arlt, J.; Henderson, R. A 100Mphoton/s time-resolved mini-silicon photomultiplier with on-chip fluorescence lifetime estimation in 0.13 μm CMOS imaging technology. In Proceedings of the 2012 IEEE International Solid-State Circuits Conference, San Francisco, CA, USA, 19–23 February 2012; pp. 122–124.
174. Niclass, C.; Favi, C.; Kluter, T.; Gersbach, M.; Charbon, E. A 128 \times 128 Single-Photon Image Sensor with Column-Level 10-Bit Time-to-Digital Converter Array. *IEEE J. Solid-State Circuits* **2008**, *43*, 2977–2989. [[CrossRef](#)]
175. Dutton, N.A.W.; Gneccchi, S.; Parmesan, L.; Holmes, A.J.; Rae, B.; Grant, L.A.; Henderson, R.K. 11.5 A time-correlated single-photon-counting sensor with 14GS/S histogramming time-to-digital converter. Proceedings of the 2015 IEEE International Solid-State Circuits Conference—(ISSCC) Digest of Technical Papers, San Francisco, CA, USA, 22–26 February 2015; pp. 1–3.
176. Di Sieno, L.; Mora, A.D.; Boso, G.; Tosi, A.; Pifferi, A.; Cubeddu, R.; Contini, D. Diffuse optics using a dual window fast-gated counter. *Appl. Opt.* **2014**, *53*, 7394–7401. [[CrossRef](#)]
177. Behera, A.; di Sieno, L.; Pifferi, A.; Martelli, F.; Mora, A.D. Instrumental, optical and geometrical parameters affecting time-gated diffuse optical measurements: A systematic study. *Biomed. Opt. Express* **2018**, *9*, 5524–5542. [[CrossRef](#)]
178. Di Sieno, L.; Boetti, N.G.; Mora, A.D.; Pugliese, D.; Farina, A.; Konugolu Venkata Sekar, S.; Ceci-Ginistrelli, E.; Janner, D.; Pifferi, A.; Milanese, D. Towards the use of bioresorbable fibers in time-domain diffuse optics. *J. Biophotonics* **2017**, *11*, e201600275. [[CrossRef](#)]
179. Pifferi, A.; Torricelli, A.; Cubeddu, R.; Quarto, G.; Re, R.; Konugolu Venkata Sekar, S.; Spinelli, L.; Farina, A.; Martelli, F.; Wabnitz, H. Mechanically switchable solid inhomogeneous phantom for performance tests in diffuse imaging and spectroscopy. *J. Biomed. Opt.* **2015**, *20*, 121304. [[CrossRef](#)] [[PubMed](#)]

180. Martelli, F.; di Ninni, P.; Zaccanti, G.; Contini, D.; Spinelli, L.; Torricelli, A.; Cubeddu, R.; Wabnitz, H.; Mazurenka, M.; Macdonald, R. Phantoms for diffuse optical imaging based on totally absorbing objects, part 2: Experimental implementation. *J. Biomed. Opt.* **2014**, *19*, 76011. [CrossRef] [PubMed]
181. Spinelli, L.; Botwicz, M.; Zolek, N.; Kacprzak, M.; Milej, D.; Sawosz, P.; Liebert, A.; Weigel, U.; Durduran, T.; Foschum, F.; et al. Determination of reference values for optical properties of liquid phantoms based on Intralipid and India ink. *Biomed. Opt. Express* **2014**, *5*, 2037–2053. [CrossRef]
182. Vavadi, H.; Mostafa, A.; Zhou, F.; Uddin, K.M.S.; Althobaiti, M.; Xu, C.; Bansal, R.; Ademuyiwa, F.; Poplack, S.; Zhu, Q. Compact ultrasound-guided diffuse optical tomography system for breast cancer imaging. *J. Biomed. Opt.* **2018**, *24*, 021203. [CrossRef]
183. Zhu, Q. Optical Tomography with Ultrasound Localization: Initial Clinical Results and Technical Challenges. *Technol. Cancer Res. Treat.* **2005**, *4*, 235–244. [CrossRef]
184. Cortese, L.; Presti, G.L.; Pagliazzi, M.; Contini, D.; Mora, A.D.; Pifferi, A.; Konugolu Venkata Sekar, S.; Spinelli, L.; Taroni, P.; Zanoletti, M.; et al. Liquid phantoms for near-infrared and diffuse correlation spectroscopies with tunable optical and dynamic properties. *Biomed. Opt. Express* **2018**, *9*, 2068–2080. [CrossRef]
185. Glycerine Producers' Association. *Physical Properties of Glycerine and Its Solutions*; Glycerine Producers' Association: New York, NY, USA, 1963.
186. Quarto, G.; Pifferi, A.; Bargigia, I.; Farina, A.; Cubeddu, R.; Taroni, P. Recipes to make organic phantoms for diffusive optical spectroscopy. *Appl. Opt.* **2013**, *52*, 2494–2502. [CrossRef]
187. SOLUS—Smart Optical and Ultrasound Diagnostics of Breast Cancer. Available online: <http://www.solus-project.eu/> (accessed on 29 November 2019).
188. LUCA—Laser and Ultrasound Co-analyzer for Thyroid Nodules. Available online: <http://luca-project.eu/> (accessed on 29 November 2019).
189. Lanka, P.; Farina, A.; Konugolu Venkata Sekar, S.; Guadagno, C.; Spinelli, L.; Taroni, P.; Cubeddu, R.; Nisoli, E.; Pifferi, A. Multidistance time domain diffuse optical spectroscopy in the assessment of abdominal fat heterogeneity. In *Biophotonics: Photonic Solutions for Better Health Care VI*; International Society for Optics and Photonics: Bellingham, WA, USA, 2018; Volume 10685, p. 1068513.
190. Farina, A.; Konugolu Venkata Sekar, S.; Guadagno, C.; Spinelli, L.; Lanka, P.; Taroni, P.; Cubeddu, R. In vivo depth heterogeneity of the abdomen assessed by broadband time-domain diffuse optical spectroscopy. *Eur. Conf. Biomed. Opt.* **2017**, *10412*, 104120M.
191. Di Sieno, L.; Cubeddu, R.; Sportouche, H.; Savéry, D.; Konugolu Venkata Sekar, S.; Rosinski, B.; Farina, A.; Ferocino, E.; Lanka, P.; Taroni, P.; et al. Solid heterogeneous phantoms for multimodal ultrasound and diffuse optical imaging: An outcome of the SOLUS project for standardization. In *Novel Biophotonics Techniques and Applications V*; International Society for Optics and Photonics: Bellingham, WA, USA, 2019; Volume 11075, p. 1107516.
192. Lanka, P.; Yang, L.; Orive-Miguel, D.; Veesa, J.D.; Tagliabue, S.; Sudakou, A.; Samaei, S.; Forcione, M.; Kovacsova, Z.; Behera, A.; et al. The BITMAP exercise: A multi-laboratory performance assessment campaign of diffuse optical instrumentation. In *Diffuse Optical Spectroscopy and Imaging VII*; International Society for Optics and Photonics: Bellingham, WA, USA, 2019; Volume 11074, p. 110741A.
193. Konugolu Venkata Sekar, S.; Pacheco, A.; Martella, P.; Li, H.; Lanka, P.; Pifferi, A.; Andersson-Engels, S. A Solid Phantom Recipe for Diffuse Optics in Biophotonics Applications: A Step Towards Anatomically Correct 3D Tissue Phantoms. *Biomed. Opt. Express* **2019**, *10*, 2090–2100.

